Geol. Mag. **149** (*4*), *2012, pp. 645–661.* © *Cambridge University Press 2011*
doi:10.1017/S0016756811000860

Sr–Nd isotopic characteristics of the Late Cretaceous Shuangyashan suite: evidence for enriched mantle 2 in Northeast China

LEI ZHANG*‡, BAO-FU HAN*†, JIA-FU CHEN* & ZHAO XU*

*Ministry of Education Key Laboratory of Orogenic Belts and Crustal Evolution, School of Earth and Space Sciences, Peking University, Beijing 100871, P. R. China
‡Institute of Geology, Chinese Academy of Geological Sciences, Beijing 100037, P. R. China

(*Received* 3 December 2009; *accepted* 2 August 2011; *first published online* 3 November 2011)

Abstract – In Northeast China, large volumes of Mesozoic–Cenozoic igneous rocks have developed as a result of long-lasting subduction of the palaeo-Pacific and Pacific plates beneath the eastern Eurasian continent. Previous studies have convincingly confirmed the presence of depleted mantle (DM), FOcal ZOne (FOZO) mantle and enriched mantle 1 (EM1) end-members; the enriched mantle 2 (EM2) end-member is probably present but it has been poorly constrained. The Late Cretaceous Shuangyashan suite, comprising a monzogabbro and diorite–porphyrite stocks and their cumulate hornblendite enclaves, from the Shuangyashan coal basin, Northeast China, is characterized by high initial $^{87}Sr/^{86}Sr$ (0.70922–0.71095) and low initial $^{143}Nd/^{144}Nd$ ratios (0.51221–0.51238) at 98 Ma. Their occurrence demonstrates that EM2 is present in the lithospheric mantle of Northeast China and its formation may be related to recycled continental material in a subduction setting.

Keywords: Sr–Nd isotopes, enriched mantle 2, subduction, Northeast China.

1. Introduction

It is well known that the mantle is heterogeneous in composition and encompasses several end-members in terms of Sr, Nd and Pb isotopes (e.g. White, 1985; Zindler & Hart, 1986). In active continental margin, fluid or melt released from subducted sediments or seawater-altered oceanic crust could significantly modify the lithospheric mantle and participate in the generation of subduction-related magma (e.g. McCulloch *et al.* 1983; Vroon *et al.* 1995; Bailey, 1996; Plank & Langmuir, 1998; Elliott, 2003; Bouvier, Métrich & Deloule, 2008). Consequently, the mantle in a subduction setting is dominated by three end-members: depleted mantle (DM) with low $^{87}Sr/^{86}Sr$ and high $^{143}Nd/^{144}Nd$ ratios; enriched mantle 1 (EM1) with low $^{87}Sr/^{86}Sr$ and low $^{143}Nd/^{144}Nd$ ratios; and enriched mantle 2 (EM2) with high $^{87}Sr/^{86}Sr$ and low $^{143}Nd/^{144}Nd$ ratios. Accordingly, the subduction-related igneous rocks have highly varied Sr–Nd isotopic compositions and usually show a DM–EM1 or a DM–EM2 trend on a Sr–Nd isotope variation diagram (e.g. Kelemen, Hanghøj & Greene, 2003).

Northeast China (Fig. 1a) on the eastern Eurasian continent has long been an active continental margin since Early Mesozoic time (e.g. Wang & Mo, 1995; Maruyama *et al.* 1997), characterized by large volumes of Mesozoic–Cenozoic igneous rocks (e.g. Liu, Han & Fyfe, 2001; Wu *et al.* 2005*a*, 2011). Previous Sr–Nd isotope studies on these igneous rocks have clearly recognized the DM end-member, as represented by the peridotite xenoliths from Wangqing (e.g. Xu *et al.* 1998) and the EM1 end-member defined by the Cenozoic basalts from Wudalianchi (e.g. Basu *et al.* 1991; Zhang *et al.* 1995; Fan, Sui & Liu, 2001; Zou *et al.* 2003). In addition, many peridotite xenoliths and Cenozoic basalts from Northeast China have higher $^{87}Sr/^{86}Sr$ ratios than EM1, indicating the possible presence of EM2, and its formation may be related to the subduction of the palaeo-Pacific and Pacific plates beneath the eastern Eurasian continent (Basu *et al.* 1991; Tatsumoto *et al.* 1992; Xu *et al.* 1998; Chen, Hsu & Ho, 2003; Choi *et al.* 2006). However, the location and the Sr–Nd isotopic characteristics of EM2 have been poorly constrained. In this study, we report the Sr–Nd isotopic compositions of the Late Cretaceous Shuangyashan suite, comprising a monzogabbro and diorite–porphyrite stocks and their hornblendite enclaves; convincingly demonstrate the presence of EM2 in Northeast China; delimit the Sr–Nd isotopic compositions of EM2; and discuss the relationship between EM2 and cycling of the subducted continental material.

2. Geological setting

Northeast China comprises several blocks, including the Palaeozoic Xing'an Block, Songliao Block and the Precambrian Jiamusi Massif from west to east (Fig. 1a). The evolution of Northeast China has involved the palaeo-Asian Ocean from Late Palaeozoic to Early Mesozoic time and the Mongol-Okhotsk Ocean from Early Mesozoic to Late Mesozoic time, followed by the subduction of the palaeo-Pacific and Pacific plates

† Author for correspondence: bfhan@pku.edu.cn

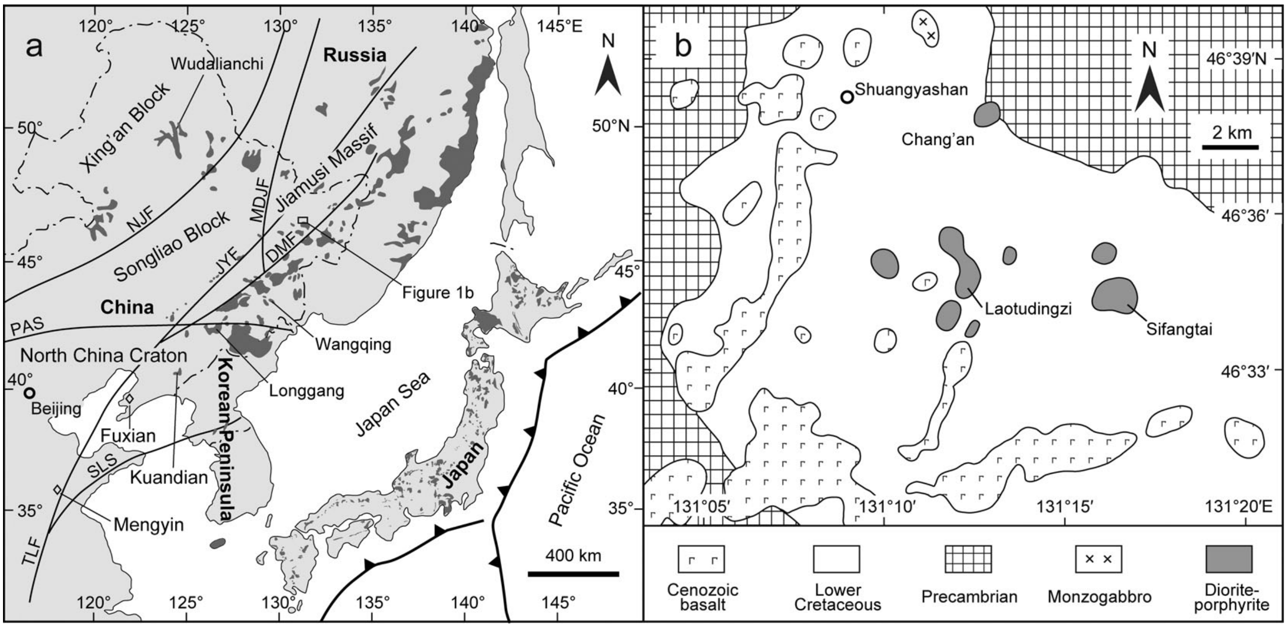

Figure 1. (a) Simplified map showing the major units, faults and distribution of Cenozoic basalts (dark grey areas) in Northeast Eurasia and the approximate location of (b). Diamonds show the locations of Fuxian and Mengyin peridotite xenoliths from the eastern North China Craton. DMF – Dunmi Fault, JYF – Jiayi Fault, MDJF – Mudanjiang Fault, NJF – Nenjiang Fault, PAS – palaeo-Asian Suture, SLS – Sulu Suture, TLF – Tanlu Fault. (b) Sketch map showing the locations of the monzogabbro and hornblendite enclave-bearing diorite–porphyrite stocks in the Shuangyashan coal basin.

from Early Mesozoic time (e.g. Wang & Mo, 1995; Zhao *et al*. 1996; Li *et al*. 2009; Wu *et al*. 2011). The long history has been accompanied by widespread development of voluminous Late Palaeozoic and Mesozoic plutons (e.g. Wu *et al*. 2000, 2005*a*, 2011; Zhang *et al*. 2004; Xu *et al*. 2008) and Cenozoic basalts (e.g. Hsu & Chen, 1998; Liu, Han & Fyfe, 2001; Zhang *et al*. 2002; Chen *et al*. 2007; Fig. 1a).

Since Early Cretaceous time, the eastern part of Northeast China had been an active continental margin (e.g. Meng & Zhou, 1996; Maruyama *et al*. 1997; Taira, 2001) before the opening of the Sea of Japan in Miocene time (Otofuji & Matsuda, 1983, 1984; Horikoshi, 1990; Jolivet, Tamaki & Fournier, 1994) and in a back-arc setting after the opening of the Sea of Japan (e.g. Wang & Mo, 1995; Liu, Han & Fyfe, 2001), during which a few Cretaceous coal basins occur in the eastern part of Northeast China, including the Shuangyashan coal basin on the Jiamusi Massif (HBGMR, 1993). The Shuangyashan basin is underlain by the Precambrian Mashan complex, which consists of amphibole schist and gneiss and underwent Middle to Late Cambrian metamorphism (e.g. Song *et al*. 1997; Li *et al*. 1999; Wilde, Zhang & Wu, 2000). The metamorphic basement is unconformably covered by the Lower Cretaceous coal-bearing Chengzihe and Muling formations, which are dominated by sandstone, mudstone and minor tuff, with abundant coal beds (HBGMR, 1993). These coal-bearing sequences are unconformably overlain by the Miocene basalts (Fig. 1b).

In the Shuangyashan basin, the Lower Cretaceous coal-bearing sequences (HBGMR, 1993) are intruded by a suite of Late Cretaceous intrusions, including one monzogabbro and eight diorite–porphyrite stocks. These intrusions are small in size (0.4–5 km^2). The monzogabbro is coeval with the diorite–porphyrites (HBGMR, 1993), and its zircon SHRIMP U–Pb age is 98 ± 2 Ma (Zhang *et al*. 2009). All the diorite–porphyrite stocks contain variable numbers of cumulate hornblendite enclaves, but large-size enclaves are only present in the Sifangtai intrusion.

Petrologically, the monzogabbro is massive and holocrystalline, showing a typical poikilitic texture (Zhang *et al*. 2009). Olivine, clinopyroxene, orthopyroxene, plagioclase, biotite and ilmenite are chadacrysts, while K-feldspar is oikocryst. The diorite–porphyrites are massive and have a porphyritic texture (Zhang *et al*. 2011). The matrix is composed of very fine-grained anhedral plagioclase and amphibole, and the phenocrysts comprise fine- to medium-grained plagioclase. Medium- to coarse-grained amphibole is also present in the diorite–porphyrites. It is pargasitic in composition, similar to that in the cumulate hornblendite enclaves, and often has embayed rims. This mineral is supposed to be a xenocryst derived from fragmented cumulate hornblendites (Zhang *et al*. 2011). The hornblendite enclaves show a typical cumulate texture: pargasitic amphibole and minor clinopyroxene are cumulus, whereas anorthitic plagioclase (An > 85 mol. %) is intercumulus. Rare biotite and ilmenite are present in the enclaves. Based on their mineralogy and element geochemistry, the enclaves are proposed to be derived from layered cumulate hornblendites in the crust–mantle transition zone, which may have crystallized from hydrous basaltic magma (Zhang *et al*. 2011).

https://doi.org/10.1017/S0016756811000860 Published online by Cambridge University Press

3. Samples and analytical methods

Most samples were collected from quarries and three (07LTDZ02, 07LTDZ04 and 07LTDZ06) were from a prospecting trench. Diorite–porphyrite and hornblendite enclave samples were mainly collected from the Sifangtai, Laotudingzi and Chang'an intrusions.

In this study, 9 samples were analysed for major oxide content and 16 for trace element concentration. Twenty-two whole-rock samples as well as K-feldspar and clinopyroxene separates from two monzogabbro samples (05SYS1 and 05SYS2) were analysed for Sr–Nd isotopic compositions. In particular, in the powder preparation for the diorite–porphyrite samples, amphibole xenocrysts were carefully removed.

Major oxide contents of whole-rock samples were determined by X-ray fluorescence (XRF) (ARL ADVANTXP+) on fused glass discs at the Ministry of Education Key Laboratory of Orogenic Belts and Crustal Evolution, Peking University in Beijing. USGS standard BCR-2 and Chinese national standard GSR-3 were used to monitor the analytical process.

Trace element concentration analyses were performed at the State Key Laboratory of Continental Dynamics, Northwest University in Xi'an, China. Samples were dissolved in acid and their trace element concentrations were measured by inductively coupled plasma mass spectrometry (ICP-MS) (Elan 6100 DRC). International standard samples BHVO-1 and AVG-1 were used to monitor the analytical process. The precision is better than 5 %. The accuracy, indicated by relative difference between measured and recommended values, is better than 2 % for most of the trace elements. The analytical procedure was detailed by Rudnick *et al*. (2004).

Sr–Nd isotopic analyses were done at the Isotopic Laboratory of the Institute of Geology and Geophysics, Chinese Academic of Science, Beijing. Sr and Nd were separated using a routine two-column ion exchange technique: one column for separation of light rare earth elements (LREEs) (1 × 8 cm, packed with Bio-Rad AG50×8, 200–400 mesh resin), and the other for purification of Nd (0.6 × 7 cm) was packed with Kel-F Teflon powder coated with an exchange medium of HDEHP. Procedural blanks were < 500 pg for Sr and < 100 pg for Nd. Sr and Nd isotopic analyses were performed on a Finnigan MAT-262 multi-collector mass spectrometer in static mode for Sr and in dynamic mode for Nd. During Sr–Nd isotopic analyses, NBS-987 Sr and JNdi Nd standards yielded $^{87}Sr/^{86}Sr$ = 0.710244 ± 0.000008 (n = 12) and $^{143}Nd/^{144}Nd$ = 0.512119 ± 0.000005 (n = 11), respectively, and BCR-2 gave $^{87}Sr/^{86}Sr$ = 0.705012 ± 0.000016 (n = 5) and $^{143}Nd/^{144}Nd$ = 0.512645 ± 0.000016 (n = 5). The measured $^{87}Sr/^{86}Sr$ and $^{143}Nd/^{144}Nd$ ratios were normalized to $^{86}Sr/^{88}Sr$ = 0.1194 and $^{146}Nd/^{144}Nd$ = 0.7219, respectively. The analytical procedures for Sr–Nd isotopes are the same as those described by Wu *et al*. (2005*b*).

4. Results

Only one hornblendite enclave has been analysed for major oxide contents and trace element concentrations in this study (Table 1). It shows similar geochemistry to the Group 2 enclaves as reported in Zhang *et al*. (2011). Three of eight diorite–porphyrite samples are from the Sifangtai intrusion and their major oxide contents and trace element concentrations are in good accordance with those previously reported by Zhang *et al*. (2011). Only trace element concentrations and Sr–Nd isotopic compositions of the monzogabbro are analysed in this study, and their major oxide contents were recently reported by Zhang *et al*. (2009). All the data presented in this study and earlier papers (Zhang *et al*. 2009, 2011) are combined together to characterize the Shuangyashan suite in the following sections.

4.a. Major oxides

The hornblendite enclaves (Table 1) are characterized by low SiO_2 (41.08–43.99 wt %) and high MgO (9.74–15.91 wt %), CaO (11.40–12.36 wt %) and TiO_2 (1.34–2.34 wt %). Total alkali contents ($Na_2O + K_2O$) and Mg no. ($= 100 \times Mg/(Mg + Fe^{2+})$) of the hornblendite enclaves vary in the range of 1.96–4.15 wt % and 62.3–74.3, respectively.

The monzogabbro and diorite–porphyrites are subalkaline (Fig. 2a) and calc-alkaline (Fig. 2b). The monzogabbro shows narrow variations in major oxide contents (SiO_2 = 51.26–51.74 wt %, Al_2O_3 = 14.16–14.75 wt %, Na_2O = 1.91–2.06 wt %, K_2O = 2.96–3.18 wt %, MgO = 7.77–8.32 wt %) and high Mg no. (65.9–67.3) and total alkali contents (4.92–5.14 wt %) (Table 1). The diorite–porphyrites have higher SiO_2 (53.13–61.38 wt %) and Al_2O_3 (17.91–19.07 wt %) and lower MgO (1.83–3.86 wt %), $Fe_2O_3^T$ (5.40–9.13 wt %) and Mg no. (42.7–49.6) than the monzogabbro, and their CaO, Na_2O and K_2O and total alkali contents vary in the ranges of 4.69–8.43 wt %, 2.32–3.27 wt %, 1.22–2.24 wt % and 3.54–5.18 wt %, respectively. Among the three diorite–porphyrite intrusions, the Chang'an intrusion has the highest MgO (3.49–3.86 wt %), $Fe_2O_3^T$ (8.57–9.13 wt %), TiO_2 (0.91–1.04 wt %), CaO (7.88–8.43 wt %) and Mg no. (48.7–49.6) and the lowest SiO_2 (53.13–53.74 wt %), Na_2O (2.32–2.49 wt %) and K_2O (1.22–1.33 wt %), whereas the Laotudingzi intrusion has the highest SiO_2 (60.27–61.38 wt %) and the lowest TiO_2 (0.58–0.60 wt %), $Fe_2O_3^T$ (5.40–6.10 wt %) and CaO (4.69–5.25 wt %) contents.

4.b. Trace elements

The hornblendite enclaves exhibit weak Nb and Ta negative anomalies, consistent U, Zr and Hf negative anomalies, and Ba and K positive anomalies (Fig. 3a). The enclaves show convex primitive mantle-normalized REE patterns (Fig. 3b), with weak Eu

Table 1. Major oxide and trace element concentrations of Shuangyashan hornblendite enclaves, monzogabbro and diorite–porphyrites

Sample Rock type Location	05SFT3-1* HE Sifangtai	05SFT4-1* HE Sifangtai	05SFT6-1* HE Sifangtai	05SFT12-1* HE Sifangtai	05SFT13-1* HE Sifangtai	07SFT01b HE Sifangtai
SiO_2	41.75	42.98	41.85	43.99	41.97	41.08
TiO_2	1.97	2.34	1.72	1.34	2.17	1.89
Al_2O_3	16.46	13.94	15.59	9.58	14.36	16.56
$Fe_2O_3{}^T$	13.73	13.93	12.34	12.84	13.05	14.18
MnO	0.18	0.18	0.17	0.17	0.18	0.16
MgO	9.74	11.69	10.83	15.91	12.44	10.05
CaO	12.28	11.42	11.61	12.36	11.40	12.12
Na_2O	1.62	1.64	3.20	1.43	1.89	1.71
K_2O	0.71	0.82	0.95	0.53	0.91	0.78
P_2O_5	0.06	0.04	0.18	0.03	0.05	0.18
LOI	1.49	0.95	1.49	1.81	1.54	0.81
Total	99.99	99.93	99.93	99.99	99.96	99.52
Mg no.	62.3	66.2	67.2	74.3	69.0	62.3
ICP-MS (μg/g)						
Be	0.52	0.66	0.65	0.35	0.66	0.52
Sc	81.8	99.7	91.8	83.0	68.8	42.7
V	711	878	827	485	384	272
Cr	68.5	69.0	153	438	2.94	285
Co	39.4	44.5	42.5	51.8	35.4	50.2
Ni	25.1	15.8	10.5	23.3	3.60	60.7
Cu	15.4	15.1	26.1	13.3	16.3	13.8
Zn	76.4	81.6	78.4	70.1	96.3	104
Ga	15.7	16.7	17.3	12.4	18.3	21.4
Rb	11.4	9.30	9.77	2.12	7.81	6.82
Sr	218	264	274	141	217	243
Y	35.4	34.9	37.9	23.6	44.4	43.7
Zr	44.1	47.0	56.1	28.3	64.9	62.6
Nb	4.32	3.96	4.33	2.43	4.70	5.00
Cs	0.31	0.28	0.37	0.24	0.74	0.14
Ba	180	190	221	86.2	142	137
La	4.67	5.38	7.36	2.22	6.78	3.92
Ce	15.7	17.8	21.0	8.62	20.7	14.5
Pr	2.54	2.99	2.94	1.43	3.13	2.69
Nd	16.1	18.8	16.3	11.3	17.4	16.0
Sm	5.28	6.14	5.04	3.93	5.37	5.41
Eu	1.52	1.82	1.39	1.14	1.52	1.38
Gd	5.99	6.92	5.90	4.40	6.58	6.15
Tb	1.06	1.15	1.08	0.76	1.22	1.05
Dy	6.68	6.98	6.80	4.46	7.71	6.46
Ho	1.35	1.38	1.43	0.93	1.65	1.39
Er	3.66	3.61	4.03	2.47	4.82	3.73
Tm	0.52	0.50	0.59	0.36	0.68	0.53
Yb	2.99	2.74	3.48	1.97	3.99	3.28
Lu	0.40	0.36	0.48	0.27	0.54	0.46
Hf	1.61	1.73	1.73	1.12	2.10	1.82
Ta	0.25	0.21	0.23	0.13	0.28	0.23
Pb	3.50	3.20	3.50	2.55	3.51	1.70
Th	0.28	0.30	0.27	0.09	0.41	0.17
U	0.09	0.08	0.13	0.05	0.10	0.08

negative anomalies ($(Eu/{}^*Eu)_N$ = 0.73–0.85) and no obvious REE fractionations ($(La/Yb)_N$ = 0.81–1.52).

The monzogabbro shows little variation in trace element concentrations (Table 1). It is characterized by enriched large-ion lithophile elements (LILEs) with respect to high-field-strength elements (HFSEs), with striking Nb, Ta and Ti negative anomalies and a weak Rb positive anomaly (Fig. 3c). The monzogabbro has Nb/U, Ce/Pb, Zr/Nb, Ba/Th, Th/La and Ba/La ratios of 2.60–3.18, 3.46–3.91, 15.8–18.2, 51.6–64.5, 0.35–0.43 and 20.8–23.1, and shows enriched light rare earth elements (LREEs) with respect to heavy rare earth elements (HREEs), with $(La/Yb)_N$ = 5.51–5.78 (Fig. 3d) and $(Eu/{}^*Eu)_N$ = 0.78–0.86.

The diorite–porphyrites are generally characterized by enriched LILEs relative to HFSEs, with Nb, Ta and Ti negative anomalies as well as a slight Sr positive anomaly (Fig. 3e). Except for 07LTDZ04, other diorite–porphyrite samples show similar LILE, LREE and HFSE but different HREE concentrations (Fig. 3e, f). The Chang'an intrusion has the highest HREE concentrations and the lowest REE fractionation ($(La/Yb)_N$ = 4.33–4.45), whereas the Laotudingzi intrusion has the lowest HREE concentrations and the highest REE fractionation ($(La/Yb)_N$ = 8.18–13.06). Two samples (07LTDZ04 and 07LTDZ06) from the Laotudingzi intrusion have slight Eu positive anomalies ($(Eu/{}^*Eu)_N$ = 1.30 and 1.05, respectively), samples from the Chang'an intrusion exhibit weak Eu negative anomalies ($(Eu/{}^*Eu)_N$ = 0.82–0.86) and those from the Sifangtai intrusion show negligible Eu negative anomalies ($(Eu/{}^*Eu)_N$ = 0.93–1.00). Generally, the three diorite–porphyrite intrusions have Nb/U and Ce/Pb ratios of 11.6–23.6 and 3.74–10.3.

Table 1. (*Cont.*)

Sample Rock type Location	SYS1† MG Shuangyashan	SYS2† MG Shuangyashan	SYS3† MG Shuangyashan	SYS4† MG Shuangyashan	SYS5† MG Shuangyashan	07SYSNE02† MG Shuangyashan	07SYSNE03† MG Shuangyashan
SiO_2	51.47	51.54	51.74	51.55	51.57	51.26	51.36
TiO_2	0.95	0.92	0.89	0.98	0.92	0.93	0.88
Al_2O_3	14.31	14.57	14.46	14.40	14.18	14.16	14.75
$Fe_2O_3{}^T$	9.65	9.35	9.28	9.37	9.20	9.42	9.08
MnO	0.15	0.15	0.15	0.15	0.14	0.15	0.14
MgO	8.18	8.03	7.95	7.77	7.90	8.32	7.97
CaO	9.63	9.72	9.81	9.34	9.63	9.72	9.79
Na_2O	1.91	1.99	2.00	1.96	2.02	1.96	2.06
K_2O	3.01	2.96	2.99	3.18	3.09	3.11	2.96
P_2O_5	0.39	0.38	0.38	0.41	0.39	0.40	0.40
LOI	0.19	0.29	0.32	0.42	0.48	0.09	0.25
Total	99.84	99.90	99.97	99.53	99.52	99.52	99.64
Mg no.	66.4	66.7	66.6	65.9	66.7	67.3	67.2
ICP-MS (μg/g)							
Be	2.31	2.45	2.48	2.75	2.62	2.40	2.53
Sc	33.9	33.5	26.3	28.5	36.9	33.2	32.7
V	200	188	200	202	217	206	199
Cr	393	384	390	366	434	408	399
Co	34.9	34.1	33.5	34.2	35.0	35.4	34.9
Ni	92.0	88.3	87.1	86.6	91.0	92.4	89.8
Cu	39.3	37.0	38.3	42.3	39.7	39.9	38.7
Zn	82.0	78.4	80.1	82.2	79.5	88.1	86.1
Ga	16.2	16.1	16.1	16.6	16.6	17.4	18.0
Rb	158	158	156	177	199	160	156
Sr	443	450	444	428	439	448	455
Y	28.3	27.9	27.7	29.2	29.4	28.5	28.0
Zr	132	123	128	134	135	126	127
Nb	7.31	7.23	7.02	8.46	7.53	7.49	7.29
Cs	8.05	7.87	8.12	10.3	11.0	8.36	9.57
Ba	443	440	443	477	504	490	442
La	19.8	20.1	19.6	20.9	22.8	21.2	21.2
Ce	44.8	45.0	45.0	48.4	51.2	47.5	47.3
Pr	5.97	6.1	6.03	6.43	6.70	6.03	5.82
Nd	25.8	26.1	25.9	27.2	29.5	26.7	25.9
Sm	5.65	5.78	5.78	6.03	6.52	6.02	5.91
Eu	1.52	1.53	1.53	1.52	1.57	1.55	1.54
Gd	5.21	5.18	5.24	5.54	5.88	5.45	5.23
Tb	0.81	0.79	0.81	0.85	0.89	0.82	0.80
Dy	4.41	4.41	4.49	4.69	4.98	4.78	4.68
Ho	0.93	0.93	0.94	0.98	1.05	1.00	0.97
Er	2.47	2.44	2.52	2.68	2.73	2.76	2.68
Tm	0.40	0.39	0.39	0.41	0.42	0.43	0.41
Yb	2.55	2.55	2.55	2.72	2.95	2.69	2.63
Lu	0.40	0.39	0.39	0.42	0.44	0.39	0.38
Hf	3.12	2.94	3.12	3.28	3.51	3.11	3.12
Ta	0.41	0.41	0.40	0.48	0.47	0.45	0.43
Pb	12.5	12.8	13.0	13.4	13.9	12.9	12.1
Th	7.82	7.83	6.87	8.79	9.76	8.58	8.23
U	2.30	2.31	2.24	2.87	2.90	2.58	2.42

4.c. Sr–Nd isotopes

All the samples are characterized by high $^{87}Sr/^{86}Sr$ and low $^{143}Nd/^{144}Nd$ ratios (Table 2). In particular, the K-feldspar and clinopyroxene separates from the monzogabbro have the same Sr–Nd isotopic compositions as the whole-rock samples (Table 2). Samples from the three diorite–porphyrite intrusions show consistent Sr–Nd isotopic compositions (Table 2). After age correction, the monzogabbro and diorite–porphyrites have the same initial $^{143}Nd/^{144}Nd$ ratios at 98 Ma: 0.51226–0.51229 for the monzogabbro and 0.51221–0.51227 for the diorite–porphyrites, respectively. However, the diorite–porphyrites have slightly higher initial $^{87}Sr/^{86}Sr$ ratios (0.71052–0.71095) than the monzogabbro (0.70943–0.70958). Comparatively, the hornblendite enclaves display relatively large variations in their initial $^{87}Sr/^{86}Sr$ and $^{143}Nd/^{144}Nd$ ratios: 0.70922–0.71073 and 0.51229–0.51238, respectively, covering the ranges of initial $^{87}Sr/^{86}Sr$ and $^{143}Nd/^{144}Nd$ ratios of the monzogabbro and diorite–porphyrites.

5. Discussion

Although the Shuangyashan suite comprises three different types of rocks, these rocks are commonly characterized by high initial $^{87}Sr/^{86}Sr$ and low initial $^{143}Nd/^{144}Nd$ ratios (Table 2), and they do not show a common evolution trend (Fig. 4), indicating that they may have crystallized from different parental magmas or been affected by crustal contamination and post-magmatic processes.

https://doi.org/10.1017/S0016756811000860 Published online by Cambridge University Press

Table 1. (*Cont.*)

Sample Rock type Location	05SFT3–2* DP Sifangtai	05SFT4–2* DP Sifangtai	05SFT6–2* DP Sifangtai	05SFT12–2* DP Sifangtai	05SFT13–2* DP Sifangtai	07SFT01a DP Sifangtai	07SFT06a DP Sifangtai
SiO_2	56.89	56.58	56.63	57.39	57.76	58.07	57.56
TiO_2	0.74	0.76	0.75	0.74	0.75	0.70	0.71
Al_2O_3	18.74	18.32	18.84	18.93	19.07	18.11	18.66
$Fe_2O_3{}^T$	6.77	6.67	6.75	6.72	6.85	6.51	6.65
MnO	0.13	0.13	0.14	0.14	0.13	0.12	0.12
MgO	2.48	2.36	2.50	2.44	2.44	2.26	2.14
CaO	7.08	7.00	7.28	7.12	7.06	6.83	7.15
Na_2O	2.60	3.03	2.68	2.74	2.74	3.00	3.27
K_2O	1.62	1.70	1.67	1.62	1.60	2.03	1.52
P_2O_5	0.28	0.30	0.28	0.29	0.29	0.27	0.28
LOI	2.67	3.12	2.42	1.86	1.26	2.27	1.75
Total	99.98	99.98	99.95	99.99	99.94	100.17	99.81
Mg no.	46.1	45.2	46.3	45.8	45.4	44.7	42.9
ICP-MS (μg/g)							
Be	1.72	1.82	1.77	1.80	1.83	2.40	2.30
Sc	11.0	11.8	11.5	10.7	11.1	13.2	13.3
V	48.2	50.9	52.2	45.1	47.6	49.2	50.3
Cr	11.6	10.2	15.0	7.99	14.2	13.0	11.6
Co	9.08	9.37	9.25	8.91	9.10	9.92	10.5
Ni	2.89	2.06	3.32	1.56	3.51	3.65	3.54
Cu	5.31	4.86	4.85	5.41	5.11	3.89	4.11
Zn	97.3	98.4	98.9	98.5	101	104	117
Ga	22.3	22.8	22.5	22.5	23.1	25.8	27.2
Rb	39.9	50.2	41.6	41.7	44.4	73.6	42.2
Sr	532	579	537	552	550	598	580
Y	26.0	26.8	25.4	26.9	27.2	28.6	28.5
Zr	151	155	148	161	162	166	168
Nb	11.4	11.6	11.5	11.6	11.7	12.3	12.5
Cs	1.39	1.50	1.46	1.54	1.79	1.46	1.00
Ba	635	635	633	605	634	629	572
La	24.1	23.6	22.8	24.5	24.5	22.3	21.2
Ce	50.4	50.0	48.2	52.1	51.5	47.4	45.2
Pr	6.37	6.23	6.09	6.51	6.52	5.88	5.62
Nd	27.1	26.8	26.1	27.6	26.7	24.6	23.7
Sm	5.57	5.60	5.42	5.60	5.42	5.00	4.89
Eu	1.62	1.67	1.69	1.63	1.67	1.46	1.48
Gd	4.84	5.03	4.93	5.02	5.06	4.60	4.45
Tb	0.76	0.78	0.76	0.78	0.76	0.67	0.67
Dy	4.35	4.44	4.25	4.29	4.36	3.92	3.89
Ho	0.89	0.94	0.88	0.89	0.88	0.83	0.82
Er	2.64	2.71	2.62	2.65	2.61	2.31	2.29
Tm	0.42	0.42	0.41	0.41	0.40	0.35	0.36
Yb	2.54	2.70	2.56	2.58	2.69	2.37	2.43
Lu	0.39	0.40	0.39	0.40	0.40	0.36	0.37
Hf	3.74	3.81	3.71	3.83	3.93	3.52	3.47
Ta	0.76	0.77	0.76	0.76	0.75	0.61	0.59
Pb	12.3	10.7	12.9	11.8	11.2	9.30	9.43
Th	3.56	3.55	3.31	3.59	3.53	3.55	3.08
U	0.78	0.80	0.73	0.80	0.69	0.74	1.08

5.a. Evaluation of crustal contamination and post-magmatic processes

It is known that crustal contamination and post-magmatic processes may have resulted in great geochemical and isotopic differences between igneous rocks and their parental magmas (e.g. Glazner & Farmer, 1992; Foland, Gibb & Henderson, 2000; Barry, Saunders & Kempton, 2003; Katzir *et al.* 2007). Hence, it is very important to evaluate whether the monzogabbro and diorite–porphyrites have been affected by crustal contamination and post-magmatic processes.

As mentioned in Section 3, all the samples were collected from a prospecting trench and quarries. They are very fresh and have no features of post-magmatic alteration in thin-section. In trace elements, highly incompatible elements such as Rb and Th are commonly mobile and compatible elements such as Hf are immobile during surface processes (e.g. Ward, McArthur & Walsh, 1992; Le Roex, Bell & Davis, 2003; Xu *et al.* 2005; Kumar, Reddy & Leelannandam, 2006). Consequently, incompatible elements may vary greatly, compared to compatible elements, during post-magmatic processes. For the Shuangyashan suite, most elements have similar and consistent correlations with Hf, except for La in sample 07LTDZ04 (Fig. 5a–d), but Rb and Th show very different correlations with Hf in individual rock types (Fig. 5e, f). The differences in Rb and Th concentrations between different rock types cannot be simply attributed to the effects of post-magmatic processes, because increasing or decreasing Rb concentrations in rocks during post-magmatic processes will enlarge or reduce the present

Table 1. (*Cont.*)

Sample Rock type Location	07SFT12 DP Sifangtai	07LTDZ02 DP Laotudingzi	07LTDZ04 DP Laotudingzi	07LTDZ06 DP Laotudingzi	07CA04 DP Chang'an	07CA05a DP Chang'an
SiO_2	57.20	60.27	61.38	60.87	53.13	53.74
TiO_2	0.72	0.60	0.58	0.59	1.04	0.91
Al_2O_3	18.27	17.91	18.19	18.12	18.51	18.70
$Fe_2O_3{}^T$	6.77	6.10	5.40	5.73	9.13	8.57
MnO	0.12	0.05	0.05	0.05	0.16	0.15
MgO	2.39	2.23	1.90	1.83	3.86	3.49
CaO	6.73	4.92	4.69	5.25	8.43	7.88
Na_2O	2.85	2.86	2.94	3.14	2.32	2.49
K_2O	1.96	1.61	2.24	1.49	1.22	1.33
P_2O_5	0.29	0.21	0.21	0.21	0.30	0.27
LOI	2.22	2.93	2.78	2.76	1.44	2.03
Total	99.52	99.69	100.36	100.04	99.54	99.56
Mg no.	45.1	46.0	45.1	42.7	49.6	48.7
ICP-MS (μg/g)						
Be	1.87	2.22	2.19	2.18	1.53	1.56
Sc	12.7	10.8	10.0	10.2	24.2	21.3
V	51.4	52.4	47.6	49.7	124	106
Cr	17.1	19.2	13.5	33.5	27.6	29.4
Co	10.3	6.32	6.73	6.66	17.2	15.7
Ni	6.00	7.31	4.14	17.0	8.92	11.6
Cu	6.14	2.70	1.64	16.6	13.4	16.0
Zn	101	37.3	33.7	37.9	105	107
Ga	23.6	24.7	24.2	25.1	22.9	23.4
Rb	58.7	66.6	88.5	54.8	30.4	33.6
Sr	541	543	623	595	458	447
Y	28.7	17.2	16.8	19.3	36.9	35.7
Zr	165	167	171	171	150	151
Nb	11.9	13.2	13.3	12.9	11.8	10.9
Cs	1.53	9.49	7.88	3.90	0.59	0.82
Ba	682	588	715	440	486	501
La	23.5	27.8	18.0	28.2	21.6	20.8
Ce	50.8	57.0	36.5	57.7	47.7	46.5
Pr	6.38	6.78	4.37	7.19	6.23	5.91
Nd	27.1	27.4	18.1	29.7	27.5	26.2
Sm	5.60	5.16	3.50	5.51	6.13	5.82
Eu	1.68	1.42	1.37	1.69	1.62	1.62
Gd	5.18	4.06	2.99	4.45	6.02	5.76
Tb	0.76	0.54	0.43	0.58	0.95	0.92
Dy	4.50	2.95	2.56	3.09	5.79	5.69
Ho	0.96	0.58	0.55	0.61	1.25	1.22
Er	2.67	1.60	1.55	1.64	3.50	3.46
Tm	0.41	0.24	0.24	0.24	0.52	0.52
Yb	2.65	1.61	1.58	1.55	3.48	3.45
Lu	0.41	0.25	0.24	0.23	0.52	0.52
Hf	3.99	4.16	4.27	4.12	3.54	3.64
Ta	0.66	0.73	0.74	0.71	0.62	0.60
Pb	12.5	8.40	5.47	5.60	8.43	9.06
Th	3.24	4.89	4.00	4.13	2.83	3.45
U	0.66	0.72	0.74	0.72	0.50	0.58

Mg no. = 100 × Mg/(Mg + Fe^{2+}); Abbreviations: HE – hornblendite enclave; MG – monzogabbro; DP – diorite–porphyrite.
* Major oxides and trace element data from Zhang *et al.* (2011).
† Major oxides data of the monzogabbro from Zhang *et al.* (2009).

$^{87}Sr/^{86}Sr$ ratios and this may lead to largely varied initial $^{87}Sr/^{86}Sr$ ratios. However, the monzogabbro and diorite–porphyrites show limited variations in their Sr–Nd isotopic compositions, especially in the initial $^{87}Sr/^{86}Sr$ ratios (Table 2), respectively. This indicates that post-magmatic processes have had little effect on the Shuangyashan suite.

Possibly, crustal contamination is another mechanism contributing to the high Sr and low Nd isotopic characteristics of the Shuangyashan suite. In this aspect, the Cretaceous cover and basement rocks of the Shuangyashan basin as well as Triassic plutons that intrude the Jiamusi Massif must be taken into consideration. Unfortunately, there are no available Sr–Nd isotopic data for the Cretaceous country rocks of the Shuangyashan suite. Three samples from the Mashan complex, which may represent the basement rocks of the Shuangyashan basin, have greatly varied Sr–Nd isotopic compositions at 100 Ma: $^{87}Sr/^{86}Sr$ = 0.70621 and $^{143}Nd/^{144}Nd$ = 0.51228 for garnet-bearing granite, $^{87}Sr/^{86}Sr$ = 0.72326 and $^{143}Nd/^{144}Nd$ = 0.51210 for adamellite, and $^{87}Sr/^{86}Sr$ = 0.73712 and $^{143}Nd/^{144}Nd$ = 0.51195 for granulite (Wu *et al.* 2000). In addition, the Triassic granites that are intruded into the Jiamusi Massif have $^{87}Sr/^{86}Sr$ and $^{143}Nd/^{144}Nd$ ratios of 0.71010–0.73273 and 0.51204–0.51212 at

https://doi.org/10.1017/S0016756811000860 Published online by Cambridge University Press

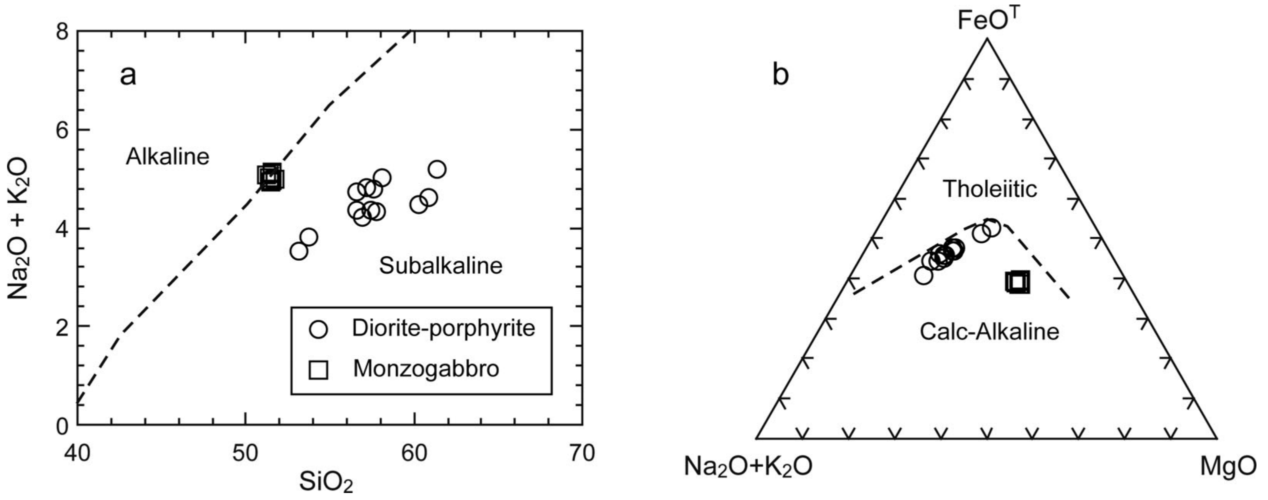

Figure 2. ($Na_2O + K_2O$)–SiO_2 (a) and ($Na_2O + K_2O$)–FeO^T–MgO (b) diagrams for the monzogabbro and diorite–porphyrites of the Shuangyashan suite, showing that the monzogabbro and diorite–porphyrites are calc-alkaline rocks. Data from Table 1 and Zhang *et al*. (2009, 2011). Boundary between tholeiitic and calc-alkaline is from Irvine & Baragar (1971).

100 Ma (Wu *et al*. 2000). Except for the garnet-bearing granite, which has an initial $^{87}Sr/^{86}Sr$ ratio significantly lower than, and an initial $^{143}Nd/^{144}Nd$ ratio similar to, the Shuangyashan suite, the other rocks have lower initial $^{143}Nd/^{144}Nd$ ratios than the Shuangyashan suite and their initial $^{87}Sr/^{86}Sr$ ratios vary greatly. Importantly, the basement rocks and Triassic granite plutons show very different trends from the diorite–porphyrites whose initial $^{87}Sr/^{86}Sr$ ratios show no changes with Sr concentrations, unlike the basement rocks and Triassic granite plutons (Fig. 6a). It seems that these rocks might have been involved in the Shuangyashan suite.

However, the monzogabbro has a low and narrow range of SiO_2 contents (51.26–51.74 wt %) and high Mg no. (65.9–67.3). This, combined with its mineralogy (Zhang *et al*. 2009), indicates that it may have crystallized from basaltic magma. In this case, any crustal contamination must have occurred during magma ascent. The monzogabbro shows little variation in major oxides and trace elements (Table 1; Figs 2, 3c, d), and its K-feldspar oikocryst and clinopyroxene chadacryst separates have the same $^{87}Sr/^{86}Sr$ and $^{143}Nd/^{144}Nd$ ratios as whole-rock samples (Table 2), suggesting that the monzogabbro is geochemically homogeneous, with little contribution from either upper crust material (SiO_2 = 66.6 wt %, Sr = 320 ppm, Rudnick & Gao, 2003) or the basement rocks and Triassic granites of the Jiamusi Massif.

Texture, mineralogy (pargasitic amphibole, anorthitic plagioclase (An > 85 mol. %) and minor clinopyroxene) and elemental geochemistry (low SiO_2 = 41.08–43.99 wt % and high Mg no. = 62.3–74.3) of the hornblendite enclaves suggest that they were derived from layered cumulate hornblendites crystallized from hydrous basaltic magma with Mg no. > 63 in the crust–mantle transition zone (Zhang *et al*. 2011). The hornblendite enclaves have initial $^{87}Sr/^{86}Sr$ and $^{143}Nd/^{144}Nd$ ratios indistinguishable from those of the monzogabbro (Table 2). They do not show any evidence for crustal contamination.

If the hornblendite enclaves were derived from the crust–mantle transition zone (Zhang *et al*. 2011), the enclave-bearing diorite–porphyrites must have had an origin at least in the crust–mantle transition zone or even in the mantle. In any case, the high SiO_2 contents (53.13–61.38 wt %) and low Mg no. (42.7–49.6) of the diorite–porphyrite may have resulted from low-degree partial melting of the mantle, fractional crystallization of mantle-derived magma or involvement of more crustal material. The diorite–porphyrites generally have slightly higher initial $^{87}Sr/^{86}Sr$ ratios (0.7105–0.7110) than the monzogabbro (0.7094–0.7096) and the hornblendite enclaves (0.7092–0.7107), but all of them have indistinguishable initial $^{143}Nd/^{144}Nd$ ratios of 0.51221–0.51238 (Table 2). This implies that the Mashan complex and Triassic granitic plutons may have contributed negligible contamination to the diorite–porphyrites. On the other hand, the diorite–porphyrites show no evident change in the initial $^{87}Sr/^{86}Sr$ ratios with increasing SiO_2 contents (Fig. 6b), suggesting a predominant fractional crystallization for the diorite–porphyrites (Figs 2, 6). This is supported by of the relationship between the initial $^{87}Sr/^{86}Sr$ ratios and 1/Sr (Fig. 6a). Among the diorite–porphyrite intrusions, the Chang'an and the Laotudingzi may have crystallized from the least- and most-evolved magmas, respectively. The former has the lowest SiO_2 and the highest $Fe_2O_3^T$, CaO and Mg no., with weaker REE fractionation ($(La/Yb)_N$ = 4.33–4.45), while the latter has the highest SiO_2 and the lowest $Fe_2O_3^T$and CaO, with stronger REE fractionation ($(La/Yb)_N$ = 8.18–13.06).

The diorite–porphyrites are coeval with the monzogabbro (HBGMR, 1993) and they show similar Sr–Nd isotopic compositions to the monzogabbro and the hornblendite enclaves. Particularly, the hornblendite enclaves completely plot over the Sr–Nd

https://doi.org/10.1017/S0016756811000860 Published online by Cambridge University Press

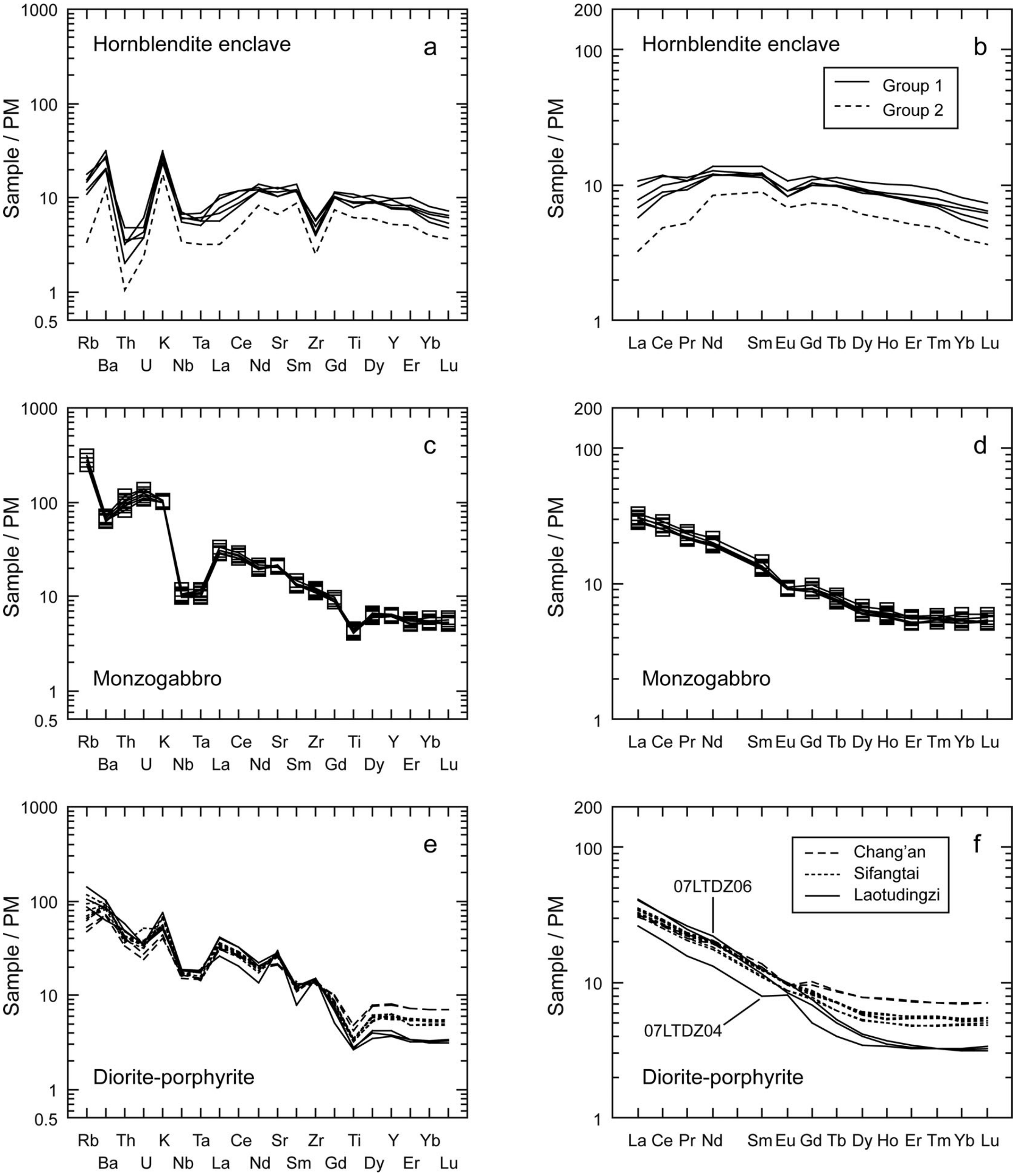

Figure 3. Primitive mantle (PM) normalized trace element and REE patterns of the hornblendite enclaves (a & b), monzogabbro (c & d), and diorite–porphyrite (e & f). Data from Table 1 and Zhang *et al*. (2011). Normalization values are from Sun & McDonough (1989).

isotopic compositions of the monzogabbro and diorite–porphyrites (Fig. 7), indicating that their Sr–Nd isotopic characteristics may have been inherited from a common source rather than contributed from crustal contamination. This common source for the Shuangyashan suite may be in the mantle, as constrained by the origin of the monzogabbro and hornblendite enclaves.

5.b. Lithospheric mantle origin for EM2

Mantle-derived magma may originate from the asthenosphere (e.g. Arndt & Christensen, 1992; Pearson & Nowell, 2002; Pearson, Canil & Shirey, 2003) or the lithosphere (e.g. Zhang *et al*. 1991; Verma, 2000; Ersoy, Helvaci & Palmer, 2010). The asthenospheric magma may interact with the overlying lithospheric mantle

https://doi.org/10.1017/S0016756811000860 Published online by Cambridge University Press

Table 2. Sr–Nd isotope analysis results for Shuangyashan hornblendite enclaves, monzogabbro, diorite–porphyrites and separates of K-feldspar and clinopyroxene from the monzogabbro

Sample	Rock type	Note	Location	$^{87}Sr/^{86}Sr$	$\pm 2\sigma$	$^{143}Nd/^{144}Nd$	$\pm 2\sigma$	$(^{87}Sr/^{86}Sr)_i$	$(^{143}Nd/^{144}Nd)_i$
05SFT3-1	HE	WR	Sifangtai	0.709429	10	0.512509	10	0.70922	0.51238
05SFT4-1	HE	WR	Sifangtai	0.710367	10	0.512345	9	0.71023	0.51229
05SFT6-1	HE	WR	Sifangtai	0.709791	9	0.512481	12	0.70965	0.51236
05SFT12-1	HE	WR	Sifangtai	0.710021	8	0.512428	11	0.70996	0.51229
05SFT13-1	HE	WR	Sifangtai	0.710040	10	0.512420	9	0.70990	0.51230
07SFT01b	HE	WR	Sifangtai	0.710843	12	0.512439	11	0.71073	0.51231
SYS1	MG	WR	Shuangyashan	0.71088	6	0.512376	13	0.70948	0.51229
SYS2	MG	WR	Shuangyashan	0.71076	3	0.512354	9	0.70943	0.51227
SYS3	MG	WR	Shuangyashan	0.71091	7	0.512349	7	0.70958	0.51226
SYS4	MG	WR	Shuangyashan	0.71112	3	0.512363	6	0.70950	0.51228
SYS5	MG	WR	Shuangyashan	0.71105	7	0.512345	6	0.70958	0.51226
05SYS1	MG	Kfs	Shuangyashan	0.711082	9	0.512339	14		
05SYS1	MG	Cpx	Shuangyashan	0.709786	9	0.512393	10		
05SYS2	MG	Kfs	Shuangyashan	0.710993	10	0.512332	13		
05SYS2	MG	Cpx	Shuangyashan	0.709770	14	0.512392	11		
05SFT3-2	DP	WR	Sifangtai	0.711187	9	0.512331	10	0.71089	0.51225
05SFT4-2	DP	WR	Sifangtai	0.711047	9	0.512347	12	0.71070	0.51227
05SFT6-2	DP	WR	Sifangtai	0.711263	9	0.512335	10	0.71095	0.51226
05SFT12-2	DP	WR	Sifangtai	0.711126	9	0.512291	12	0.71082	0.51221
05SFT13-2	DP	WR	Sifangtai	0.711201	14	0.512320	12	0.71088	0.51224
07SFT01a	DP	WR	Sifangtai	0.711389	10	0.512304	15	0.71089	0.51226
07SFT06a	DP	WR	Sifangtai	0.711202	11	0.512325	12	0.71091	0.51225
07LTDZ02	DP	WR	Laotudingzi	0.711240	10	0.512327	11	0.71075	0.51225
07LTDZ04	DP	WR	Laotudingzi	0.711087	9	0.512332	12	0.71052	0.51226
07CA04	DP	WR	Chang'an	0.711088	13	0.512304	11	0.71082	0.51222
07CA05a	DP	WR	Chang'an	0.711215	13	0.512318	13	0.71091	0.51223

In initial $^{87}Sr/^{86}Sr$ and $^{143}Nd/^{144}Nd$ calculation, $^{87}Rb/^{86}Sr$ and $^{147}Sm/^{144}Nd$ values were calculated from Rb, Sr, Sm and Nd concentrations of whole-rock samples measured by ICP-MS as reported in Table 1 and Zhang *et al.* (2011). Abbreviations: HE – hornblendite enclave; MG – monzogabbro; DP – diorite–porphyrite; WR – whole rock; Kfs – K-feldspar; Cpx – clinopyroxene.

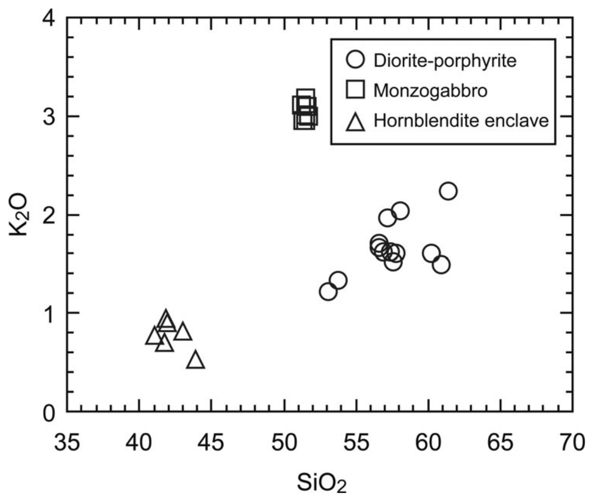

Figure 4. K_2O–SiO_2 diagram showing that the monzogabbro, diorite–porphyrites and hornblendite enclaves of the Shuangyashan suite may have crystallized from different parental magma. Data from Table 1 and Zhang *et al.* (2009, 2011).

during its upward transportation (Ellam & Cox, 1991; Xu *et al.* 2005). In this case, the asthenospheric magma could be modified by the lithospheric mantle and show some lithospheric mantle affinity (Ellam & Cox, 1991; Xu *et al.* 2005). Similarly, the lithospheric mantle could be refertilized by the asthenospheric magma and shows some geochemical features of the asthenosphere (e.g. Saal *et al.* 2001; Le Roux *et al.* 2007; Ersoy, Helvaci & Palmer, 2010; van Acken *et al.* 2010).

Oceanic basalts (ocean island basalt (OIB) and mid-ocean ridge basalt (MORB)) may be derived from asthenospheric mantle and have little interaction with the lithospheric mantle during their upward transportation so that they show asthenospheric geochemical affinity, and some element ratios such as Ce/Pb and Nb/U can be used to detect their source regions (e.g. Pearce, Harris & Tindle, 1984; Hofmann *et al.* 1986; Hofmann, 1988; Zou *et al.* 2003; Xu *et al.* 2005). It is generally accepted that the average Ce/Pb and Nb/U ratios for oceanic basalts (OIB and MORB) are 25 ± 5 and 47 ± 7, respectively (Hofmann *et al.* 1986). For the Shuangyashan suite, trace element ratios of the diorite–porphyrites may have been largely modified owing to significant fractional crystallization (Fig. 6) and thus they cannot be used to identify the origin for mantle-derived magma. The Ce/Pb and Nb/U ratios of the monzogabbro are 3.46–3.91 and 2.60–3.18, respectively, significantly lower than those of oceanic basalts (Fig. 8a, b). In addition, other element ratios such as Zr/Nb (15.8–18.2), Ba/Th (51.6–64.5), Th/La (0.35–0.43) and Ba/La (20.8–23.1) of the monzogabbro are very different from those of oceanic basalts but similar to continental crust (Weaver, 1991). It seems that the monzogabbro does not have asthenospheric mantle affinity, or its parental magma is derived from the asthenosphere but involves continental material. If its mineralogy and tectonic setting are taken into consideration, the monzogabbro, together with the diorite–porphyrites and their hornblendite enclaves, is more possibly derived from the lithospheric mantle.

It is generally accepted that the upper mantle is composed of upper spinel- and lower garnet-facies

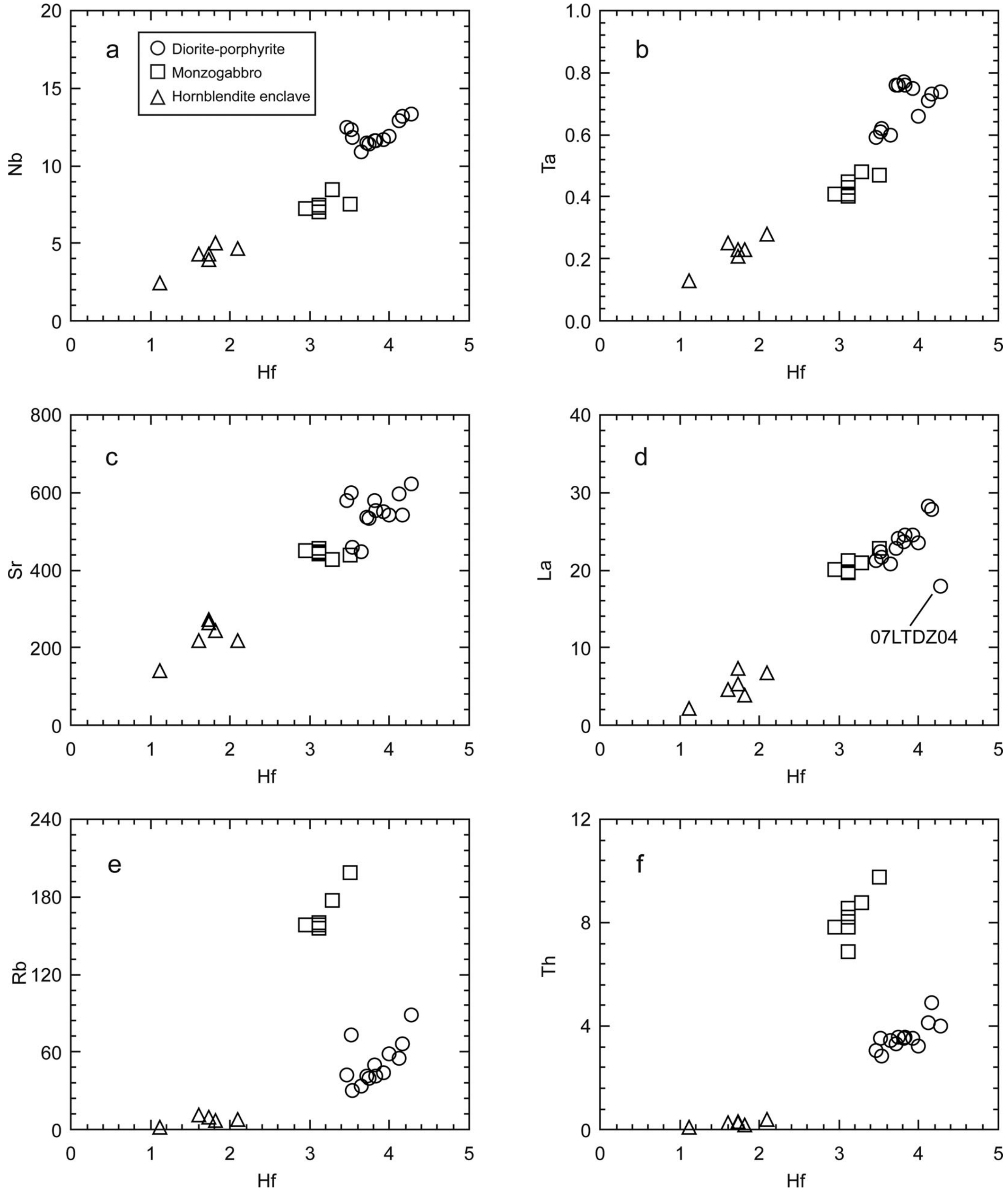

Figure 5. Selected trace elements versus Hf diagrams for the Shuangyashan suite. Data from Table 1 and Zhang *et al*. (2011). The Shuangyashan suite seems to show a differentiation trend (a–d) but different trends in highly incompatible elements Rb and Th (e & f), indicating that surface processes have no effect on the rocks and there is no evolutionary relationship between different types of rocks.

peridotite, and the spinel–garnet facies transition occurs at ~75 km (McKenzie & O'Nions, 1991). Geophysical studies have revealed that the present lithosphere–asthenosphere boundary below the Jiamusi Massif lies at about ~80–100 km (An & Shi, 2006; Liu *et al*. 2006; Zhang *et al*. 2006), suggesting the presence of garnet peridotite in the lower lithospheric mantle and underlying asthenosphere. Because HREEs are highly compatible and LREEs are incompatible in garnet (e.g. Shimizu & Kushiro, 1975; van Westrenen, Blundy & Wood, 1999), partial melt of garnet peridotite may be characterized by high REE fractionation, and its $(La/Yb)_N$ will decrease with increasing partial melting of garnet peridotite: $(La/Yb)_N = 10$ at 20 %

https://doi.org/10.1017/S0016756811000860 Published online by Cambridge University Press

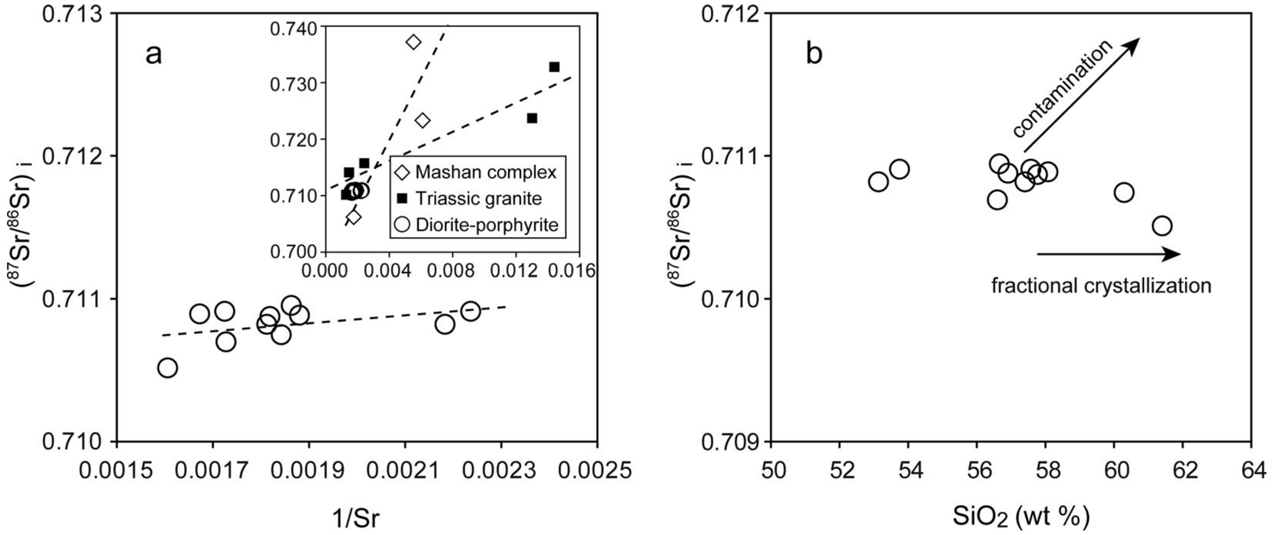

Figure 6. (^{87}Sr/^{86}Sr)$_i$–1/Sr (a) and (^{87}Sr/^{86}Sr)$_i$–SiO_2 (b) diagrams showing that the diorite–porphyrites show no obvious changes in the initial ^{87}Sr/^{86}Sr ratios as Sr and SiO_2 contents increase, suggesting a predominant fractional crystallization rather than crustal contamination. It is noted that the diorite–porphyrites show a very different trend from the Precambrian Mashan complex and Triassic granites (Wu *et al*. 2000) as shown in the inset of (a).

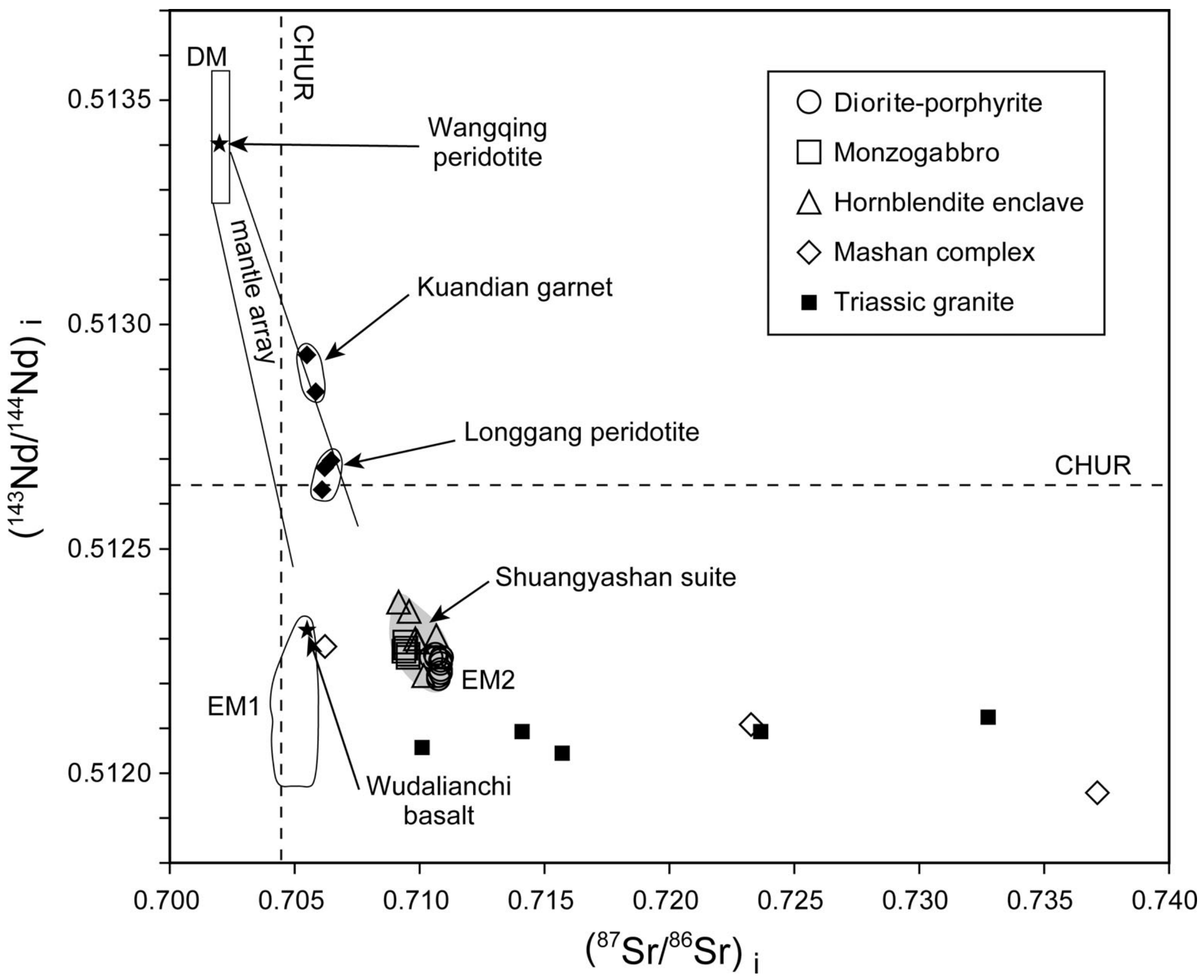

Figure 7. The Shuangyashan suite has distinct initial ^{87}Sr/^{86}Sr and ^{143}Nd/^{144}Nd ratios in comparison with the most depleted clinopyroxene separate from a Wangqing peridotite xenolith with ^{87}Sr/^{86}Sr = 0.7022 and ^{143}Nd/^{144}Nd = 0.5134 (Xu *et al*. 1998), and the most enriched Wudalianchi basalt with Sr–Nd isotopic compositions of ^{87}Sr/^{86}Sr = 0.7055 and ^{143}Nd/^{144}Nd = 0.5123 (Zhang *et al*. 1995) in Northeast China. Three Longgang peridotite xenoliths (Hsu, Chen & Ho, 2000) and Kuandian garnet megacrysts (Tatsumoto *et al*. 1992) with enriched Sr–Nd isotopic compositions are plotted near the DM–EM2 trend. The DM and EM1 ranges and mantle array lines are based on figure 6 in Zindler & Hart (1986). CHUR – chondritic uniform reservoir.

https://doi.org/10.1017/S0016756811000860 Published online by Cambridge University Press

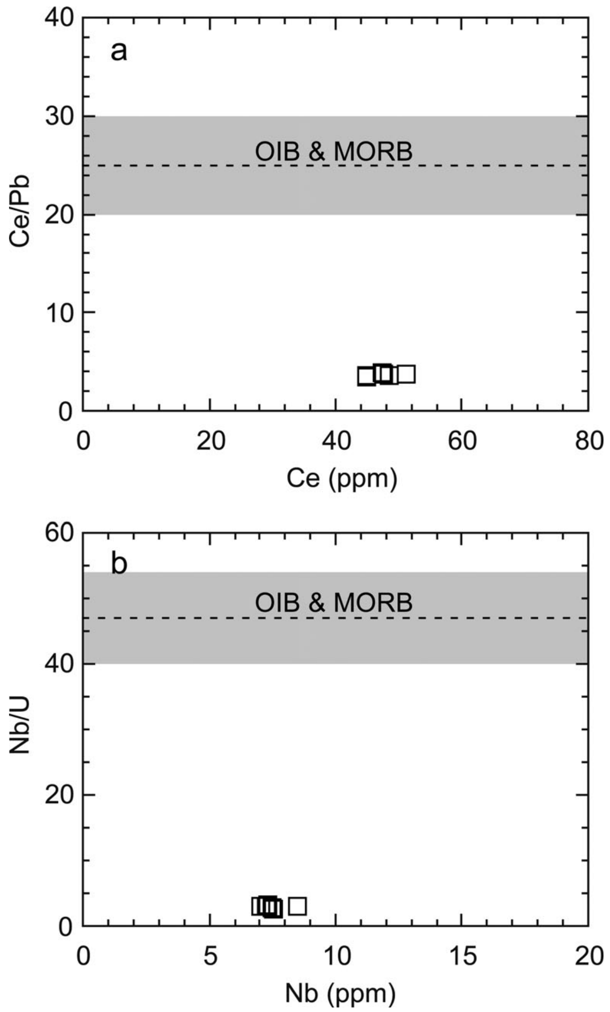

Figure 8. Ce/Pb–Ce (a) and Nb/U–Nb (b) diagrams for the monzogabbro, showing its parental magma is impossibly derived from the asthenosphere. The average Ce/Pb and Nb/U ratios in OIB and MORB are after Hofmann *et al.* (1986).

partial melting and $(La/Yb)_N$ = 50 at 5 % partial melting (Kelemen, Yogodzinski & Scholl, 2003). In the Shuangyashan suite, the monzogabbro shows moderate REE fractionation: $(La/Yb)_N$ = 5.51–5.78 (Fig. 3d). Petrography and high Mg no. of the monzogabbro suggest that only minor fractional crystallization of olivine and clinopyroxene occurred in the parental magma (Zhang *et al.* 2009). Combined with the partition coefficients (e.g. Shimizu, Sangen & Masuda, 1982; Jones & Layne, 1997; Blundy & Dalton, 2000; Bedard, 2005), the fractional crystallization of olivine and clinopyroxene will lead to rising $(La/Yb)_N$ of the residual melt. This implies that the parental magma of the monzogabbro should have very low $(La/Yb)_N$. If it was derived from the asthenosphere or lower lithospheric mantle, much more than 20 % partial melting is required and this seems impossible.

Alternatively, the parental magma of the monzogabbro was derived from partial melting of the spinel peridotite in the upper lithospheric mantle. If so, the lithospheric mantle must be characterized by enriched geochemical features. In fact, some peridotite xenoliths from Longgang ($^{87}Sr/^{86}Sr$ = 0.7060–0.7064, $^{143}Nd/^{144}Nd$ = 0.51263–0.51269; Hsu, Chen & Ho, 2000) and mantle-derived garnet megacrysts from Kuandian ($^{87}Sr/^{86}Sr$ = 0.7055–0.7058, $^{143}Nd/^{144}Nd$ = 0.51285–0.51293; Tatsumoto *et al.* 1992) (Fig. 1a) show more enriched Sr–Nd isotopic features than FOcal ZOne (FOZO) mantle and DM and significantly deviate from the DM–EM1 trend and are closer to the DM–EM2 trend (Fig. 7), implying that the enriched lithospheric mantle is probably present in Northeast China. Enriched lithospheric mantle with extremely variable $^{87}Sr/^{86}Sr$ (0.7025–0.7224) and $^{143}Nd/^{144}Nd$ (0.5094–0.5174) ratios is also present beneath the Siberian Craton (Pearson *et al.* 1995). Similarly, the Fuxian and Mengyin peridotite xenoliths from the eastern North China Craton (Fig. 1a) also show extremely variable initial $^{87}Sr/^{86}Sr$ (0.7030–0.7196) and $^{143}Nd/^{144}Nd$ (0.5120–0.5125) ratios (Zhang *et al.* 2008). Both of the examples imply the presence of enriched lithospheric mantle beneath the continents.

The Shuangyashan suite is mainly characterized by high $^{87}Sr/^{86}Sr$ and low $^{143}Nd/^{144}Nd$ ratios, being consistent with the Sr–Nd isotopic geochemistry of EM2. This, combined with the published data, suggests that EM2, in addition to DM, FOZO and EM1, is also present in the lithospheric mantle beneath Northeast China.

5.c. Genesis of EM2

The enriched signatures of the lithospheric mantle could have resulted from metasomatism by enriched fluids or melts (Ikeda, Nagao & Kagami, 2001; Xu *et al.* 2003; Senda, Tanaka & Suzuki, 2007; Scambelluri, van Roermund & Pettke, 2010), and the formation of EM2 is usually attributed to the involvement of recycled continental materials in the mantle (e.g. Saunders *et al.* 1988; Jackson *et al.* 2007; Willbold & Stracke, 2010). In a subduction setting, continent-derived trench sediments are easy to recycle into the mantle as the oceanic slab is being subducted. Particularly, seawater-altered oceanic crust and/or subducted sediments may release enriched fluids or generate enriched melts (e.g. McCulloch *et al.* 1983; Hergt *et al.* 1989; Elliott, 2003; Jackson *et al.* 2007). Usually, seawater has a higher $^{87}Sr/^{86}Sr$ ratio than oceanic crust (Veizer *et al.* 1999; Prokoph, Shields & Veizer, 2008), and consequently seawater-altered oceanic crust may have significantly increased $^{87}Sr/^{86}Sr$ ratios (e.g. Hart *et al.* 1999; Elliott, 2003). However, the $^{87}Sr/^{86}Sr$ ratio of the Cretaceous seawater was below 0.7084 (Veizer *et al.* 1999; Prokoph, Shields & Veizer, 2008), much lower than the initial $^{87}Sr/^{86}Sr$ ratios of the Shuangyashan suite. Therefore, the Sr–Nd isotopic signatures of the parental magma and the mantle source for the Shuangyashan suite cannot be simply attributed to contributions from seawater-altered oceanic crust. Alternatively, subducted sediments may be responsible

https://doi.org/10.1017/S0016756811000860 Published online by Cambridge University Press

for the EM2 isotopic signatures of the parental magmas for the Shuangyashan suite and their mantle source.

Generally, the Sr–Nd isotopic compositions of subducted sediments exhibit a great variation (Plank & Langmuir, 1998). Generally, continent-derived sediments have high $^{87}Sr/^{86}Sr$ and low $^{143}Nd/^{144}Nd$ ratios; the incorporation of subducted sediments in magma generation could greatly elevate the $^{87}Sr/^{86}Sr$ ratios of the arc magma and lower the $^{143}Nd/^{144}Nd$ ratios (e.g. Lin, 1992; Bailey, 1996; Plank & Langmuir, 1998). This is in agreement with the observation that subducted sediments from continental arcs have higher $^{87}Sr/^{86}Sr$ ratios than those from island arcs (Plank & Langmuir, 1998). Consequently, subduction-related igneous rocks may have greater or lesser EM2 signatures (e.g. McCulloch *et al*. 1983; Hergt *et al*. 1989; Vroon *et al*. 1995; Bouvier, Métrich & Deloule, 2008) and probably show a DM–EM2 trend (Hergt *et al*. 1989; Kelemen, Hanghøj & Greene, 2003; Jackson *et al*. 2007). Evidently, subducted sediments dominated by continental material may have resulted in igneous rocks with EM2 signatures by participating in the generation of magma (Jackson *et al*. 2007; Willbold & Stracke, 2010). The Sr–Nd isotopic and trace element geochemistry of the Shuangyashan suite clearly suggests that recycled continental material may have played an important role in the formation of EM2 in the lithosphere.

Tectonically, a continental arc occurred along the eastern edge of the Eurasian continent before the Japanese islands were rifted away from the Eurasian continent during Early Miocene time (e.g. Jolivet, Tamaki & Fournier, 1994; Wang & Mo, 1995; Maruyama *et al*. 1997). The detritus derived from erosion of the continental arc might have been transported into the trench and moved together with the subducting oceanic slab into the mantle, and finally participated in the generation of subduction-related magma at depth. The rising magma may have contained plenty of fluids; its interaction with the overlying lithospheric mantle may finally have given rise to significantly increased $^{87}Sr/^{86}Sr$ and decreased $^{143}Nd/^{144}Nd$ ratios as well as enrichment of LILEs and HFSEs in the lithospheric mantle. Afterwards, partial melts of the enriched lithospheric mantle may have ascended into the crust–mantle transition zone to form the layered cumulate hornblendites. Subsequently, some batches of melts may have captured fragments of the layered cumulate hornblendites and carried them into the upper crust to form the enclave-bearing diorite–porphyrites, and others may have directly ascended into the upper crust to form the monzogabbro. Therefore, the Shuangyashan suite may be representative of EM2 in the lithospheric mantle of Northeast China.

6. Conclusions

The Shuangyashan suite from Northeast China includes a monzogabbro and diorite–porphyrites and their cumulate hornblendite enclaves. Different types of rocks originated from a common source in the lithospheric mantle, and petrology and geochemistry indicate that post-magmatic processes and crustal contamination may have played a negligible role in the Sr–Nd isotopic compositions of the Shuangyashan suite. The Shuangyashan suite is characterized by high initial $^{87}Sr/^{86}Sr$ (0.70922–0.71095) and low $^{143}Nd/^{144}Nd$ ratios (0.51221–0.51238) at 98 Ma, suggesting the presence of EM2 in the lithospheric mantle beneath Northeast China. The formation of EM2 in the lithospheric mantle may be related to the participation of recycled continental material in arc magma generation and the interaction between rising magma and the overlying lithospheric mantle in a subduction setting.

Acknowledgements. Mark B. Allen and another anonymous reviewer are greatly thanked for their helpful and constructive comments and suggestions, which have greatly helped us to improve our presentation and discussion. We are grateful to Xiao-ming Liu, Ye Liu and Chao-feng Li for their help in chemical and isotopic analyses. This work was financially supported by China Geological Survey (Grant No. 1212010050502) and President's Foundation for Undergraduate Research of Peking University.

References

AN, M. J. & SHI, Y. L. 2006. Lithospheric thickness of the Chinese continent. *Physics of the Earth and Planetary Interiors* **159**, 257–66.

ARNDT, N. T. & CHRISTENSEN, U. 1992. The role of lithospheric mantle in continental flood volcanism: thermal and geochemical constraints. *Journal of Geophysics Research* **97**, 10967–81.

BAILEY, J. C. 1996. Role of subducted sediments in the genesis of Kurile-Kamchatka island arc basalts: Sr isotopic and elemental evidence. *Geochemical Journal* **30**, 289–321.

BARRY, T. L., SAUNDERS, A. D. & KEMPTON, P. D. 2003. Petrogenesis of Cenozoic basalts from Mongolia: asthenospheric versus metasomatized lithospheric mantle sources. *Journal of Petrology* **44**, 55–91.

BASU, A. R., WANG, J. W., HUANG, W. K., XIE, G. H. & TATSUMOTO, M. 1991. Major element, REE, and Pb, Nd and Sr isotopic geochemistry of Cenozoic volcanic rocks of eastern China: implications for their origin from suboceanic-type mantle reservoirs. *Earth and Planetary Science Letters* **105**, 149–69.

BEDARD, J. 2005. Partitioning coefficients between olivine and silicate melts. *Lithos* **83**, 394–419.

BLUNDY, J. & DALTON, J. 2000. Experimental comparison of trace element partitioning between clinopyroxene and melt in carbonate and silicate systems, and implications for mantle metasomatism. *Contributions to Mineralogy and Petrology* **139**, 356–71.

BOUVIER, A. S., MÉTRICH, N. & DELOULE, E. 2008. Slab-derived fluids in the magma sources of St. Vincent (Lesser Antilles Arc): volatile and light element imprints. *Journal of Petrology* **49**, 1427–48.

CHEN, J. C., HSU, C. N. & HO, K. S. 2003. Geochemistry of Cenozoic volcanic rocks and related ultramafic xenoliths from the Jilin and Heilongjiang provinces, northeast China. *Journal of Asian Earth Sciences* **21**, 1069–84.

CHEN, Y., ZHANG, Y. X., GRAHAM, D., SU, S. G. & DENG, J. F. 2007. Geochemistry of Cenozoic basalts and mantle xenoliths in Northeast China. *Lithos* **96**, 100–26.

CHOI, S. H., MUKASA, S. B., KWON, S. T. & ANDRONIKOV, A. V. 2006. Sr, Nd, Pb and Hf isotopic compositions of late Cenozoic alkali basalts in South Korea: evidence for mixing between the two dominant asthenospheric mantle domains beneath East Asia. *Chemical Geology* **232**, 134–51.

ELLAM, R. M. & COX, K. G. 1991. An interpretation of Karoo picrite basalts in terms of interaction between asthenospheric magmas and the mantle lithosphere. *Earth and Planetary Science Letters* **105**, 330–42.

ELLIOTT, T. 2003. Tracers of slab. In *Inside the Subduction Factory* (ed. J. Eiler), pp. 23–46. American Geophysical Union, Monograph vol. 138. Washington, DC, USA.

ERSOY, E. Y., HELVACI, C. & PALMER, M. R. 2010. Mantle source characteristics and melting models for the early-middle Miocene mafic volcanism in Western Anatolia: implications for enrichment processes of mantle lithosphere and origin of K-rich volcanism in post-collisional settings. *Journal of Volcanology and Geothermal Research* **198**, 112–28.

FAN, Q. C., SUI, J. L. & LIU, R. X. 2001. Sr-Nd isotopic geochemistry and magmatic evolutions of Wudalianchi volcano, Tianchi volcano and Tengchong volcano. *Acta Petrologica et Mineralogica* **20**, 233–8 (in Chinese with English abstract).

FOLAND, K. A., GIBB, F. G. F. & HENDERSON, C. M. B. 2000. Patterns of Nd and Sr isotopic ratios produced by magmatic and post-magmatic processes in the Shiant Isles Main Sill, Scotland. *Contributions to Mineralogy and Petrology* **139**, 655–71.

GLAZNER, A. & FARMER, G. L. 1992. Production of isotopic variability in continental basalts by cryptic crustal contamination. *Science* **233**, 72–4.

HART, S. R., BLUSZTAJN, J., DICK, H. J. B., MEYER, P. S. & MUEHLENBACHS, K. 1999. The fingerprint of seawater circulation in a 500-meter section of ocean crust gabbros. *Geochimica et Cosmochimica Acta* **63**, 4059–80.

HBGMR (HEILONGJIANG BUREAU OF GEOLOGY AND MINERAL RESOURCES). 1993. *Regional geology of Heilongjiang Province*. Beijing: Geological Publishing House, 734 pp. (in Chinese with English abstract).

HERGT, J. M., CHAPPELL, B. W., MCCULLOCH, M. T., MCDOUGALL, I. & CHIVAS, A. R. 1989. Geochemical and isotopic constraints on the origin of the Jurassic dolerites of Tasmania. *Journal of Petrology* **84**, 841–83.

HOFMANN, A. W. 1988. Chemical differentiation of the earth: the relationship between mantle continental crust and oceanic crust. *Earth and Planetary Science Letters* **90**, 297–314.

HOFMANN, A. W., JOCHUM, K. P., SEUFERT, M. & WHITE, W. M. 1986. Nb and Pb in oceanic basalts: new constraints on mantle evolution. *Earth and Planetary Science Letters* **79**, 33–45.

HORIKOSHI, E. 1990. Opening of the Sea of Japan and Kuroko deposit formation. *Mineralium Deposita* **25**, 140–5.

HSU, C. N. & CHEN, J. C. 1998. Geochemistry of late Cenozoic basalts from Wudalianchi and Jingpohu areas, Heilongjiang Province, northeast China. *Journal of Asian Earth Science* **16**, 385–405.

HSU, C. N., CHEN, J. C. & HO, K. S. 2000. Geochemistry of Cenozoic volcanic rocks from Kirin Province, northeast China. *Geochemical Journal* **34**, 33–58.

IKEDA, Y., NAGAO, K. & KAGAMI, H. 2001. Effects of recycled materials involved in a mantle source beneath the southwest Japan arc region: evidence from noble gas, Sr, and Nd isotopic systematics. *Chemical Geology* **175**, 509–22.

IRVINE, T. N. & BARAGAR, R. A. 1971. A guide to the chemical classification of the common volcanic rocks. *Canadian Journal of Earth Sciences* **8**, 523–48.

JACKSON, M. G., HART, S. R., KOPPERS, A. A. P., STAUDIGEL, H., KONTER, J., BLUSZTAJN, J., KURZ, M. & RUSSELL, J. A. 2007. The return of subducted continental crust in Samoan lavas. *Nature* **488**, 684–7.

JOLIVET, L., TAMAKI, K. & FOURNIER, M. 1994. Japan Sea, opening history and mechanism: a synthesis. *Journal of Geophysical Research* **99**, 22237–59.

JONES, R. H. & LAYNE, G. D. 1997. Minor and trace element partitioning between pyroxene and melt in rapidly cooled chondrules. *American Mineralogist* **82**, 534–45.

KATZIR, Y., LITVINOVSKY, B. A., JAHN, B. M., EYAL, M., ZANVILEVICH, A. N., VALLEY, J. W., VAPNIK, YE., BEERI, Y. & SPICUZZA, M. J. 2007. Interrelations between coeval mafic and A-type silicic magmas from composite dykes in a bimodal suite of southern Israel, northernmost Arabian–Nubian Shield: geochemical and isotope constraints. *Lithos* **97**, 336–64.

KELEMEN, P. B., HANGHØJ, K., & GREENE, A. R. 2003. One view of the geochemistry of subduction-related magmatic arcs, with an emphasis on primitive andesite and lower crust. In *The Crust* (ed. R. L. Rudnick), pp. 593–659. *Treatise on Geochemistry*, vol. 3 (eds H. D. Holland & K. K. Turekian). Oxford: Elsevier-Pergamon.

KELEMEN, P. B., YOGODZINSKI, G. M. & SCHOLL, D. W. 2003. Along-strike variation in the Aleutian Island Arc: Genesis of high Mg# andesite and implications for continental crust. In *Inside the Subduction Factory* (ed. J. Eiler), pp. 223–76. American Geophysical Union, Monograph vol. 138. Washington, DC, USA.

KUMAR, K. V., REDDY, M. N. & LEELANNANDAM, C. 2006. Dynamic melting of the Precambrian mantle: evidence from rare earth elements of the amphiboles from the Nellore-Khammam Schist Belt, South India. *Contributions to Mineralogy and Petrology* **152**, 243–56.

LE ROEX, A. P., BELL, D. R. & DAVIS, P. 2003. Petrogenesis of Group I kimberlites from Kimberley, South Africa: evidence from bulk-rock geochemistry. *Journal of Petrology* **44**, 2261–86.

LE ROUX, V., BODINIER, J. L., TOMMASI, A., ALARD, O., DAUTRIA, J. M., VAUCHEZ, A. & RICHES, A. J. V. 2007. The lherz spinel lherzolite: refertilized rather than pristine mantle. *Earth and Planetary Science Letters* **259**, 599–612.

LI, J. Y., NIU, B. G., SONG, B., XU, W. X., ZHANG, Y. H. & ZHAO, Z. R. 1999. *Crustal Formation and Evolution of Northern Changbai Mountains, Northeast China*. Beijing: Geological Publishing House, 137 pp. (in Chinese).

LI, J. Y., ZHANG, J., YANG, T. N., LI, Y. P., SUN, G. H., ZHU, Z. X. & WANG, L. J. 2009. Crustal tectonic division and evolution of the Southern part of the North Asian Orogenic Region and its adjacent areas. *Journal of Jilin University (Earth Science Edition)* **39**, 584–605 (in Chinese with English abstract).

LIN, P. N. 1992. Trace element and isotopic characteristics of western Pacific pelagic sediments: implications for the petrogenesis of Mariana Arc magmas. *Geochimica et Cosmochimica Acta* **56**, 1641–54.

LIU, J. Q., HAN, J. T. & FYFE, W. S. 2001. Cenozoic episodic volcanism and continental rifting in northeast China and possible link to Japan Sea development as revealed from K-Ar geochronology. *Tectonophysics* **339**, 385–401.

LIU, G. X., ZHANG, Z. H., HAN, J. T. & TANG, J. H. 2006. Features of the electric structure of the lithosphere beneath the Hinggan-Inner Mongolia and Jilin-Heilongjiang regions. *Geology in China* **33**, 824–31 (in Chinese with English abstract).

MARUYAMA, S., ISOZAKI, Y., KIMURA, G. & TERABAYASHI, M. 1997. Paleogeographic maps of the Japanese Islands: plate tectonic synthesis from 750 Ma to the present. *Island Arc* **6**, 121–42.

MCCULLOCH, M. T., JAQUES, A. L., NELSON, D. R. & LEWIS, J. D. 1983. Nd and Sr isotopes in kimberlites and lamproites from Western Australia: an enriched mantle origin. *Nature* **302**, 400–3.

MCKENZIE, D. P. & O'NIONS, R. K. 1991. Partial melt distributions from inversion of rare earth element concentrations. *Journal of Petrology* **32**, 1021–91.

MENG, Q. L. & ZHOU, Y. X. 1996. The formation and evolution of magma for J_2-K_1 volcanic-intrusive complex in Eastern Yanbian, Jilin Province. *Acta Petrologica et Mineralogica* **15**, 30–9 (in Chinese with English abstract).

OTOFUJI, Y. I. & MATSUDA, T. 1983. Paleomagnetic evidence for the clockwise rotation of Southwest Japan. *Earth and Planetary Science Letters* **62**, 349–59.

OTOFUJI, Y. I. & MATSUDA, T. 1984. Timing of rotational motion of Southwest Japan inferred from paleomagnetism. *Earth and Planetary Science Letters* **63**: 373–82.

PEARCE, J. A., HARRIS, N. B. W. & TINDLE, A. G. 1984. Trace-element discrimination diagrams for the tectonic interpretation of granitic-rocks. *Journal of Petrology* **25**, 956–83.

PEARSON, D. G., CANIL, D. & SHIREY, S. B. 2003. Mantle samples included in volcanic rocks: xenoliths and diamonds. In *The mantle and Core* (ed. R. W. Carlson), pp. 171–275. *Treatise on Geochemistry*, vol. 2 (eds H. D. Holland & K. K. Turekian). Oxford: Elsevier-Pergamon.

PEARSON, D. G. & NOWELL, G. M. 2002. The continental lithospheric mantle: characteristics and significance as a mantle reservoir. *Philosophical Transactions of the Royal Society of London* **360**, 2383–410.

PEARSON, D. G., SHIREY, S. B., CARLSON, R. W., BOYD, F. R., POKHILENKO, N. P. & SHIMIZU, N. 1995. Re-Os, Sm-Nd, and Rb-Sr isotope evidence for thick Archaean lithospheric mantle beneath the Siberian craton modified by multistage metasomatism. *Geochimica et Cosmochimica Acta* **59**, 959–77.

PLANK, T. & LANGMUIR, C. H. 1998. The chemical composition of subducting sediment and its consequences for the crust and mantle. *Chemical Geology* **145**, 325–94.

PROKOPH, A., SHIELDS, G. A. & VEIZER, J. 2008. Compilation and time-series analysis of a marine carbonate δ^{18}O, δ^{13}C, ^{87}Sr/^{86}Sr and δ^{34}S database through Earth history. *Earth Science Reviews* **87**, 113–33.

RUDNICK, R. L. & GAO, S. 2003. Composition of the continental crust. In *The Crust* (ed. R. L. Rudnick), pp. 1–64. *Treatise on Geochemistry*, vol. 3 (eds H. D. Holland & K. K. Turekian). Oxford: Elsevier-Pergamon.

RUDNICK, R. L., GAO, S., LING, W. L., LIU, Y. S. & MCDONOUGH, M. F. 2004. Petrology and geochemistry of spinel peridotite xenoliths from Hannuoba and Qixia, North China craton. *Lithos* **77**, 609–37.

SAAL, A. E., TAKAZAWA, E., FREY, F. A., SHIMIZU, N. & HART, S. R. 2001. Re-Os isotopes in the Horoman peridotite: evidence for refertilization? *Journal of Petrology* **42**, 25–37.

SAUNDERS, A. D., NORRY, M. J. & TARNEY, J. 1988. Origin of MORB and chemical-depleted mantle reservoirs: trace element constraints. *Journal of Petrology* **Special Volume 1**, 415–45.

SCAMBELLURI, M., VAN ROERMUND, H. L. M. & PETTKE, T. 2010. Mantle wedge peridotites: fossil reservoirs of deep subduction zone processes. Inferences from high and ultrahigh-pressure rocks from Bardane (Western Norway) and Ulten (Italian Alps). *Lithos* **120**, 186–201.

SENDA, R., TANAKA, T. & SUZUKI, K. 2007. Os, Nd, and Sr isotopic and chemical compositions of ultramafic xenoliths from Kurose, SW Japan: implications for contribution of slab-derived material to wedge mantle. *Lithos* **95**, 229–42.

SHIMIZU, N. & KUSHIRO, I. 1975. The partitioning of rare earth elements between garnet and liquid at high pressures: preliminary results. *Geophysical Research Letters* **2**, 413–6.

SHIMIZU, H., SANGEN, K. & MASUDA, A. 1982. Experimental-study on rare-earth element partitioning in olivine and clinopyroxene formed at 10 and 20 kb for basaltic systems. *Geochemical Journal* **16**, 107–17.

SONG, B., LI, J. Y., NIU, B. G. & XU, W. X. 1997. Single grain zircon ages and its implications in biotite-plagioclase gneiss in Mashan Group in the eastern Heilongjiang. *Acta Geoscientia Sinica* **18**, 306–12 (in Chinese with English abstract).

SUN, S. S. & MCDONOUGH, W. F. 1989. Chemical and isotopic systematics of oceanic basalts: implications for mantle composition and processes. In *Magmatism in the Ocean Basins* (eds A. D. Saunders & M. J. Norry), pp. 313–45. Geological Society of London, Special Publication no. 42.

TAIRA, A. 2001. Tectonic evolution of the Japanese island arc system. *Annual Review of Earth Planetary Sciences* **29**, 109–34.

TATSUMOTO, M., BASU, A. R., HUANG, W. K., WANG, J. W. & XIE, G. H. 1992. Sr, Nd, and Pb isotopes of ultramafic xenoliths in volcanic rocks of Eastern China: enriched components EMI and EMII in subcontinental lithosphere. *Earth and Planetary Science Letters* **113**, 107–28.

VAN ACKEN, D., BECKER, H., HAMMERSCHMIDT, K., WALKER, R. J. & WOMBACHER, F. 2010. Highly siderophile elements and Sr-Nd isotopes in refertilized mantle peridotites – a case study from the Totalp ultramafic body, Swiss Alps. *Chemical Geology* **276**, 257–68.

VAN WESTRENEN, W., BLUNDY, J. & WOOD, B. 1999. Crystal-chemical controls on trace element partitioning between garnet and anhydrous silicate melt. *American Mineralogist* **84**, 838–47.

VEIZER, J., ALA, D., AZMY, K., BRUCKSCHEN, P., BUHL, D., BRUHN, F., CARDEN, G. A. F., DIENER, A., EBNETH, S., GODDERIS, Y., JASPER, T., KORTE, C., PAWELLEK, F., PODLAHA, O. G. & STRAUSS, H. 1999. ^{87}Sr/^{86}Sr, δ^{13}C and δ^{18}O evolution of Phanerozoic seawater. *Chemical Geology* **161**, 59–88.

VERMA, S. P. 2000. Geochemical evidence for a lithospheric source for magmas from Los Humeros caldera, Puebla, Mexico. *Chemical Geology* **164**, 35–60.

VROON, P. Z., BERGEN, M. J. V., KLAVER, G. J. & WHITE, W. M. 1995. Strontium, neodymium, and lead isotopic and trace-element signatures of the East Indonesian sediments: provenance and implications for Banda Arc magma genesis. *Geochimica et Cosmochimica Acta* **59**, 2573–98.

WANG, H. Z. & MO, X. X. 1995. An outline of the tectonic evolution of China. *Episodes* **18**, 6–16.

WARD, C. D., MCARTHUR, J. M. & WALSH, J. N. 1992. Rare earth element behavior during evolution and alternation of the Dartmoor Granite, SW England. *Journal of Petrology* **33**, 785–815.

WEAVER, B. L. 1991. The origin of ocean island basalt end-member compositions: trace element and isotopic constraints. *Earth and Planetary Science Letters* **104**, 381–97.

WHITE, W. M. 1985. Source of oceanic basalts: radiogenic isotopic evidence. *Geology* **13**, 115–8.

WILDE, S. A., ZHANG, X. Z. & WU, F. Y. 2000. Extension of a newly identified 500 Ma metamorphic terrane in North East China: further U-Pb SHRIMP dating of the Mashan Complex, Heilongjiang Province, China. *Tectonophysics* **328**, 115–30.

WILLBOLD, M. & STRACKE, A. 2010. Formation of enriched mantle components by recycling of upper and lower continental crust. *Chemical Geology* **276**, 188–97.

WU, F. Y., JAHN, B. M., WILDE, S. & SUN, D. Y. 2000. Phanerozoic crustal growth: U-Pb and Sr-Nd isotopic evidence from the granites in northeastern China. *Tectonophysics* **328**, 89–113.

WU, F. Y., LIN, J. Q., WILDE, S. A., ZHANG, X. Q. & YANG, J. H. 2005*a*. Nature and significance of the Early Cretaceous giant igneous event in eastern China. *Earth and Planetary Science Letters* **233**, 103–19.

WU, F. Y., SUN, D. Y., GE, W. C., ZHANG, Y. B., GRANT, M. L., WILDE, S. A. & JAHN, B. M. 2011. Geochronology of the Phanerozoic granitoids in northeastern China. *Journal of Asian Earth Sciences* **41**, 1–30.

WU, F. Y., YANG, J. H., WILDE, S. A. & ZHANG, X. O. 2005*b*. Geochronology, petrogenesis and tectonic implications of Jurassic granites in the Liaodong Peninsula, NE China. *Chemical Geology* **221**, 127–56.

XU, Y. G., MA, J. L., FREY, F. A., FEIGENSON, M. D. & LIU, J. F. 2005. Role of lithosphere-asthenosphere interaction in the genesis of Quaternary alkali and tholeiitic basalts from Datong, western North China Craton. *Earth and Planetary Science Letters* **224**, 247–71.

XU, Y. G., MENZIES, M. A., THIRLWALL, M. F., HUANG, X. L., LIU, Y. & CHEN, X. M. 2003. “Reactive” harzburgites from Huinan, NE China: Products of the lithosphere-asthenosphere interaction during lithospheric thinning? *Geochimica et Cosmochimica Acta* **67**, 487–505.

XU, Y. G., MENZIES, M. A., VROON, P., MERCIER, J. C. & LIN, C. Y. 1998. Texture-temperature-geochemistry relationships in the upper mantle as revealed from spinel peridotite xenoliths from Wangqing, NE China. *Journal of Petrology* **39**, 469–93.

XU, W. L., PEI, F. P., GAO, F. H., YANG, D. B. & BU, Y. J. 2008. Zircon U-Pb age from basement granites in Yishu Graben and its tectonic implications. *Earth Science – Journal of China University of Geosciences* **33**, 145–50 (in Chinese with English abstract).

ZHANG, Z. C., FENG, C. Y., LI, Z. N., LI, S. C., XIN, Y., LI, Z. M. & WANG, X. Z. 2002. Petrochemical study of the Jingpohu Holocene alkali basaltic rocks, northeastern China. *Geochemical Journal* **36**, 133–53.

ZHANG, H. F., GOLDSTEIN, S. L., ZHOU, X. H., SUN, M., ZHENG, J. P. & CAI, Y. 2008. Evolution of subcontinental lithospheric mantle beneath eastern China: Re–Os isotopic evidence from mantle xenoliths in Paleozoic kimberlites and Mesozoic basalts. *Contributions to Mineralogy and Petrology* **155**, 271–93.

ZHANG, L., HAN, B. F., WEI, C. J. & SHU, G. M. 2011. Cumulate hornblendite enclaves in diorite–porphyrite intrusions from the Shuangyashan, Northeast China, and implications for the transition from lower crust to upper mantle in subduction setting. *International Journal of Earth Sciences* **100**, 63–79.

ZHANG, L., HAN, B. F., ZHU, Y. F., XU, Z., CHEN, J. F. & SONG, B. 2009. Geochronology, mineralogy, crystallization process and tectonic implications of the Shuangyashan monzogabbro in eastern Heilongjiang Province. *Acta Petrologica Sinica* **25**, 577–87 (in Chinese with English abstract).

ZHANG, M., MENZIES, M. A., SUDDABY, P. & THIRLWALL, M. F. 1991. EM1 signature from within the post-Archaean subcontinental lithospheric mantle: isotopic evidence from the potassic volcanic rocks in NE China. *Geochemical Journal* **25**, 387–98.

ZHANG, M., SUDDABY, P., THOMPSON, R. N., THIRLWALL, M. F. & MENZIES, M. A. 1995. Potassic volcanic rocks in NE China: geochemical constraints on mantle source and magma genesis. *Journal of Petrology* **36**, 1275–303.

ZHANG, Y. B., WU, F. Y., WILDE, S. A., ZHAI, M. G., LU, X. P. & SUN, D. Y. 2004. Zircon U-Pb ages and tectonic implications of ‘Early Paleozoic’ granitoids at Yanbian, Jilin Province, northeast China. *Island Arc* **13**, 484–505.

ZHANG, X. J., YANG, B. J., WU, F. Y. & LIU, G. X. 2006. The lithosphere structure in the Hingmong-Jihei (Hinggan-Mongolia-Jilin-Heilongjiang) region, northeast China. *Geology in China* **33**, 816–23 (in Chinese with English abstract).

ZHAO, C. J., PENG, Y. J., DANG, Z. X. & ZHANG, Y. P. 1996. *Tectonic Framework and Crust Evolution of Eastern Jilin and Heilongjiang Provinces*. Shenyang: Liaoning University Press, 124 pp. (in Chinese).

ZINDLER, A. & HART, S. R. 1986. Chemical geodynamics. *Annual Review of Earth and Planetary Sciences* **14**, 493–571.

ZOU, H. B., REID, M. R., LIU, Y. S., YAO, Y. P., XU, X. S. & FAN, Q. C. 2003. Constraints on the origin of historic potassic basalts from northeast China by U-Th disequilibrium data. *Chemical Geology* **200**, 189–201.